Theoretical Approaches to Soft Matter Systems

Fabrice Thalmann

Université de Strasbourg

Institut Charles Sadron

UPR 22 CNRS

23 rue du Loess, F-67034 Strasbourg Cedex

`http ://www-ics.u-strasbg.fr`

Theoretical Approaches to Soft Matter Systems
Approches théoriques pour les systèmes de matière molle

Habilitation à Diriger des Recherches

présentée par

Fabrice THALMANN

Maître de Conférences, UFR Physique et Ingéniérie
Université de Strasbourg, section n°28 du CNU

Soutenue le 18 Novembre 2010 devant le jury :

Paul Chaikin	Professeur New-York University	examinateur
Georg Maret	Professeur Université de Constance	examinateur
Carlos Marques	Directeur de Recherche CNRS Strasbourg	garant
Jörg Baschnagel	Professeur Université de Strasbourg	rapporteur
Bertrand Fourcade	Professeur UJF Grenoble	rapporteur
Josep Bonet-Avalos	Professeur URV Tarragona	rapporteur

2 Octobre 2010

Avant-Propos

Je remercie Carlos Marques d'avoir accepté de se porter garant de mon diplôme d'Habilitation à Diriger des Recherches, et de m'avoir accueilli dans la nouvelle équipe M^3, suite à la disparition du Laboratoire de Dynamique des Fluides Complexes (LFDC). Je remercie également la direction de l'Institut Charles Sadron de nous avoir accueilli en son sein, ce qui m'a permis de bénéficier d'un environnement pluridisciplinaire stimulant dans tous les domaines, aussi bien théoriques qu'expérimentaux, de la physico-chimie de la matière molle. Les travaux présentés dans ce manuscrit doivent beaucoup à mes coauteurs : Jean Farago, Nam-Kyung Lee, Albert Johner, André Schroder, Vladimir Baulin, Carlos Mendoza. Ces travaux n'auraient pas été rédigés aussi rapidement si je n'avais pu bénéficier de deux années de délégation auprès du CNRS, qui m'ont aussi permis d'explorer de nombreuses pistes en lien avec mon projet de recherche. Je remercie pour cela Thierry Charitat et Hendrik Meyer pour leurs conseils relatifs à ma demande de délégation et à ce manuscrit d'habilitation. Je remercie Jean Wolff grace à qui le volet équilibre de phases du projet de recherche a pu voir le jour. Je remercie enfin les membres du jury, et tout particulièrement les rapporteurs, d'avoir accepté de participer à l'évaluation de ce travail.

C'est avec impatience que j'attends de pouvoir d'aborder les thèmes de recherche esquissés dans ce manuscrit.

F.T., Strasbourg, le 1^{er} Octobre 2010.

Table des matières

Chapitre 1

Introduction en français

1.1 Présentation du manuscrit

Ce manuscrit d'habilitation présente au lecteur plusieurs résultats obtenus depuis mon arrivée à l'Institut Charles Sadron à la fin de l'année 2005. Recruté sur un profil de biophysique en 2001, je travaillais auparavant sur des aspects de la prédiction statistique des structures secondaires des acides ribonucléiques (ARN). Mon arrivée à l'Institut a marqué le commencement d'une activité de recherche consacrée à la physique de la matière molle, et a démarré au sein d'une équipe émergente que nous avons appelé M^3, acronyme récursif signifiant M^3 :*Membranes et Microforces*. Jusqu'à présent, cette équipe s'est concentrée sur l'étude des forces de surface et des systèmes de membranes autoassemblées. La phénoménologie représente une part substantielle des efforts de modélisation, mais des thématiques théoriques indépendantes sont aussi développées.

Ce manuscrit présente une sélection de sept articles et manuscrits suivis d'un bref projet de recherche. Les sept articles, à l'exception des deux premiers, portent sur des sujets distincts et indépendants. Trois thèmes dominants emergent cependant, regroupés sous les dénominations *Algorithmes*, *Colloides* et *Physique d'inspiration biologique*. Chaque article ou manuscrit est présenté en quelques pages qui résument les idées et résultats essentiels, et qui replacent dans leur contexte ces travaux. Un chapitre final *Perspectives* décrit les prolongements éventuels de chacun de ces résultats, et met en évidence leurs liens réciproques.

Le premier thème est *Algorithmes*. Il porte sur des méthodes de simulation pertinentes pour la physique de la matière molle. Des méthodes algébriques sont utilisées pour décrire de façon approchée les dynamiques stochastiques sur des intervalles de temps courts, fournissant de la sorte des algorithmes de simulation numérique. Le second thème est *Colloides*. Le dénominateur commun des deux résultats décrits dans ce chapitre est de modéliser la dynamique de systèmes de billes superparamagnétiques. Le dernier thème est *Physique d'inspiration biologique*. Il est impossible d'ignorer combien les sciences de la vie ont influencé, et d'une certaine façon inspiré, l'activité de recherche contemporaine en physique statistique de la matière molle. Les trois résultats présentés dans ce chapitre sont inspirés par des considérations biologiques, sans toutefois prétendre décrire pour l'instant ces phénomènes biologiques de façon réaliste.

Un chapitre intitulé *Physique statistique de mélanges phospholipides et dynamique de membrane* décrit les actuelles et futures orientations possibles de mon activité de recherche.

Les résultats de ce manuscrit d'habilitation sont rédigés en anglais. La section qui suit donne la traduction des titres et des résumés des sept articles sélectionnés, soumis ou publiés entre les années 2007 et 2010. Une version française du projet de recherche est présentée au chapitre 8.

1.2 Titres et résumés des travaux présentés

(1) Obtention par la méthode de Trotter d'algorithmes pour la dynamique Brownienne et la dynamique dissipative de particules (DPD)

F. Thalmann and J. Farago, Journal of Chemical Physics 127, 124109 (2007).
Texte reproduit page 77.

Cet article porte sur la discrétisation temporelle de la dynamique de Langevin et sur diverses procédures d'intégration numérique qui en résultent. A partir d'une méthode basée sur l'exponentiation d'opérateurs dépendant du temps, nous obtenons une méthode numérique pour la dynamique de Langevin qui s'avère équivalente à Ermak et Buckholz, *J.Comput.Phys 35, p169 (1980)*, et pas seulement la version stochastique de l'algorithme de Verlet. Cependant, nous avons vérifié par simulation que les deux méthodes donnent des résultats similaires, et partagent le même degré de précision d'ordre deux au sens faible. Nous appliquons ensuite la même stratégie pour obtenir et tester deux méthodes numériques pour la dynamique dissipative de particules (DPD). La prémière d'entre elle est compétitive, en terme de précision et de vitesse, avec les meilleurs algorithmes du moment.

(2) Algorithmes rapides pour les processus classiques de réaction-diffusion $X \to 0$

F. Thalmann and N.-K. Lee, Journal of Chemical Physics 130, 074102 (2009)
Texte reproduit page 99.

Le formalisme de Doi traite les processus de réaction-diffusion comme un problème à N corps quantique. Nous utilisons ce formalisme de seconde quantification comme point de départ pour obtenir une méthode numérique afin de simuler les processus de réaction-diffusion $X \to 0$, suivant une procédure bien établie de discrétisation temporelle. Dans le cas d'une zone de réaction localisée dans l'espace des configurations, cette formulation procure un moyen systématique pour établir un algorithme optimisé, à échelle de temps multiple, qui consacre l'essentiel du temps de calcul à explorer les configurations où la réaction est supposée se produire.

(3) Interaction ligand-récepteur dans les chaînes de colloides : lorsque les réactions sont limitées par la diffusion de rotation.

N.-K. Lee, A. Johner, F. Thalmann, L. Cohen-Tannoudji, E. Bertrand, J. Beaudry, J. Bibette and C.M. Marques, Langmuir 24, p1296-1307 (2008).
Texte reproduit page 113.

Nous discutons la théorie des interactions ligand-récepteur entre deux colloides en libre rotation maintenus à portée. Ces réactions, limitées par la diffusion de rotation, se produisent dans les suspensions de billes magnétiques où les billes sont mises au contact au moyen d'un champ magnétique appliqué, formant alors des structures alignées. En combinant la théorie de la réaction-diffusion, des simulations numériques et des arguments qualitatifs, nous calculons le temps requis pour que se produise une capture dans un certain nombre de limites pertinentes pour l'expérience. Nous trouvons dans tous les cas que le temps requis pour que la réaction se produise est supérieur au temps de rotation caractéristique du mouvement diffusif τ_{rot}. Lorsque les colloides transportent un seul ligand et un nombre n de récepteurs, nous trouvons que le temps de réaction, en unité τ_{rot}, est une fonction simple de n et de la surface relative α occupée par un domaine réactif $\alpha = \pi r_C^2/(4\pi r^2)$, où r_C est le rayon de capture ligand-récepteur et r le rayon du colloide.

(4) Accroissement de la séparation par cisaillement d'agrégats superparamagnétiques

C. Mendoza, C.M. Marques and F. Thalmann, submitted.
Texte reproduit page 127.

Nous étudions les principes de conception de la plus simple hélice colloidale, une architecture construite à partir de quatre billes identiques qui peuvent coupler rotation et translation pour induire une migration contrôlée. En considérant des billes superparamagnétiques, nous montrons que l'action simultanée d'un champ magnétique et d'un écoulement de cisaillement conduit au déplacement de l'agrégat dans la direction de la vorticité. Nous explorons la dépendance de la vitesse de migration en fonction des paramètres géométriques de l'agrégat, et trouvons que des migrations significatives peuvent être obtenues dans les conditions typiques de fonctionnement des dispositifs microfluidiques.

(5) Organisation spatiale de microtubules induite par les collisions

V.A. Baulin, C.M. Marques, F. Thalmann, Biophysical Chemistry 128, p231-244 (2007).
Texte reproduit page 133.

Le comportement dynamique de microtubules en solution peut-être fortement modifié par les interactions avec les parois ou d'autres structures. Nous examinons ici un modèle de croissance où l'accroissement en taille de l'extrémité plus est perturbée par les collisions avec d'autres microtubules. Nous montrons que ce mécanisme simple de croissance contrainte peut induire des structures ordonnées et des motifs à partir d'une suspension initialement isotrope et homogène. Les microtubules s'organisent dans un premier temps sous forme de domaines orientés aléatoirement qui grossissent et se concurrencent. En imposant ne serait-ce qu'un faible biais orientationel, les forces externes comme la gravité où les parois de cellule peuvent modifier la distribution des domaines, conduisant en fin de compte à une orientation macroscopique de l'échantillon.

(6) Un modèle schématique pour l'affinité et l'association moléculaire avec des variables d'Ising

F. Thalmann, European Physical Journal E 31, p441-454 (2010).
Texte reproduit page 151.

Après avoir discuté la pertinence de la physique statistique dans les phénomènes de reconnaissance moléculaire, nous présentons un modèle schématique d'association ligand-récepteur basée sur une chaîne d'Ising. Nous discutons les comportements possibles de l'affinité lorsque la raideur du ligand augmente. Nous considérons aussi le cas de récepteurs flexibles. Nous obtenons un échantillon de comportements intéressants, et en particulier une modulation de l'affinité induite par le durcissement ou l'assouplissement d'une liaison. L'affinité d'un ligand pour son récepteur se révèle dépendante du profil de rigidité, et nous envisageons la possibilité de coder l'information dans le profil de rigidité autant qu'avec la forme. Une étude systématique de la sélectivité des motifs de longueur $n < 8$ est menée. Le lien avec d'autres modèles de spin, et particulier les verres de spin est mentionnée en conclusion.

(7) Adhésion d'une bicouche lipide sur un tapis dilué d'ADN : analyse théorique de la déformation de la membrane résultant d'une seule chaîne polymère greffée.

F. Thalmann, V. Billot and C.M. Marques, submitted
Texte reproduit page 169.

Nous considérons une chaîne polymère greffée isolée couverte par une membrane en contact avec une surface plane et rigide, dans le contexte de l'adhésion de membranes supportées sur des surfaces portant une brosse de polymères peu dense. La membrane fluide adhère à la surface à cause des interactions non spécifiques attractives. La présence d'une macromolécule s'oppose localement au contact de la membrane

avec la surface, et déforme celle-ci. Nous donnons une estimation d'échelle à la fois de la taille et de l'élévation de la déformation de la membrane, en fonction du module de courbure, de la tension de surface, de l'énergie d'adhésion et du rayon de gyration de la chaîne, conduisant à des régimes distincts de confinement. Nous proposons également une prédiction quantitative, autocohérente appropriée pour les décollements superficiels. Des formes réalistes sont calculées qui pourraient se révéler observables sous des conditions de faible adhésion.

Chapter 2

Introduction

This Habilitation Dissertation presents to the reader several results obtained since 2005, when I joined the Institut Charles Sadron. Hired on a biophysics position in 2001, I had been previously working on some aspects of the statistical predictions of RNA secondary structures. My arrival at the Institute marked the beginning of a research activity dedicated to soft matter physics, and started within an emerging team that we named M^3, a recursive acronym standing for M^3:*Membrane and Microforces*. The team effort has been mainly on the theoretical and experimental studies of surface forces and self-assembled membrane systems. Our theoretical contributions ranged from a close interpretation and modeling of the experimental results to more thoretical subjects.

This manuscript presents a selection of seven articles and manuscripts, followed by a brief research project. All seven papers, except the two first ones, focus on distinct and somewhat unrelated subjects. Three dominant themes have emerged, however, grouped under the respective denominations of *Algorithms*, *Colloids* and *Bioinspired physics*. Each article or manuscript is introduced by a few pages summarizing the main ideas and results, and replacing the work in its context. A final chapter *Perspectives* gives a few possible future directions for each paper, and highlights their mutual connections.

The first subject is *Algorithms*. It focuses on simulation methods relevant to soft matter physics. Algebraic methods are used to approximate the stochastic dynamics on short time intervals, resulting in algorithms for numerical simulations. The second subject is *Colloids*. The common denominator of the two results appearing in this chapter involves the dynamics of superparamagnetic colloidal beads. The last subject is *Bioinspired physics*. It is impossible to ignore how much life sciences have influenced, and to some extent inspired, the current research activity in statistical physics of soft condensed matter. The three results presented in this chapter have been inspired by biological considerations, though they do not pretend to describe realistic biological processes so far.

Finally, chapter 7, entitled *Statistical physics of phospholipid mixtures and membrane dynamics*, outlines a few present and future directions of research.

Part I

Selected Results obtained at Institut Charles Sadron, Strasbourg

Chapter 3

Algorithms

3.1 Algorithms for Brownian molecular dynamics simulations

F. Thalmann and J. Farago
Trotter derivation of algorithms for Brownian and dissipative particle dynamics Journal of Chemical Physics 127, 124109 (2007), reprinted on page 77.

Abstract: This paper focuses on the temporal discretization of the Langevin dynamics, and on different resulting numerical integration schemes. Using a method based on the exponentiation of time dependent operators, we carefully derive a numerical scheme for the Langevin dynamics, that we found equivalent to the proposal of Ermak and Buckholz, *J.Comput.Phys 35, p169 (1980)*, and not simply to the stochastic version of the velocity-Verlet algorithm. However, we checked on numerical simulations that both algorithms give similar results, and share the same "weak order two" accuracy. We then apply the same strategy to derive and test two numerical schemes for the dissipative particle dynamics (DPD). The first one of them was found to compare well, in terms of speed and accuracy, with the best currently available algorithms.

Stochastic dynamics for soft matter systems

Numerical simulations offer invaluable insights on the dynamics of soft matter systems (polymers, colloids, amphiphiles). Coarse-grained models have been proposed that make it possible to address physical phenomena taking place on mesoscopic time and length scales, still beyond the possibilities of atomistic models. For instance, coarse-grained approaches to self-assembled phospholipid membranes, reviewed in [1, 2], are currently subject to intense focus [3, 4, 2, 5]. Coarse-grained models group clusters of atoms into *beads* subject to effective interaction potentials. In order to be realistic, their dynamics must account for Brownian stochasticity, and treat properly solvent mediated forces such as hydrodynamic interactions. Dissipative particle dynamics (DPD) was introduced [6, 7, 8] with the purpose of meeting these requirements. Langevin dynamics accounts well for thermal disorder but cannot describe the hydrodynamics. It nevertheless remains a useful approach in soft matter physics.

DPD randomly exchanges momentum between pairs of molecules. This momentum conservation ensures in return a regular hydrodynamic behavior of the corresponding fluid on sufficiently large scales [7]. Both shear and elongational viscosity coefficients can be associated to a molecular fluid obeying DPD, though there is by no means a simple correspondence between the naked, microscopic parameters behind the dynamics and the effective, macroscopic viscosity coefficients.

Langevin dynamics is numerically faster than Newtonian molecular dynamics (simulations are done with larger time steps) and can be used whenever hydrodynamic effects are unimportant, such as in the relaxation dynamics of polymer melts (see *e.g.* [9]).

Let us define explicitly these two dynamical schemes:

- **Langevin dynamics** of a single particle with position $\boldsymbol{r}$ and momentum $\boldsymbol{p}$

$$\dot{\boldsymbol{r}} = \frac{\boldsymbol{p}}{m} \; ; \; \dot{\boldsymbol{p}} = \boldsymbol{f}(\boldsymbol{r}(t)) - \gamma \boldsymbol{p}(t) + \sigma \boldsymbol{\psi}(t), \tag{3.1}$$

where $\boldsymbol{f}$ is an external force acting on the particle (neighboring particles or fields), γ a friction coefficient (homogeneous to a frequency), T the temperature of the thermostat, $\sigma = \sqrt{2m\gamma k_B T}$, and $\boldsymbol{\psi}(t)$ a white noise with unit variance (the derivative of a Wiener process) : $\langle \psi_\alpha(t) \rangle = 0$, $\langle \psi_\alpha(t)\psi_\beta(t') \rangle = \delta_{\alpha,\beta}\delta(t-t')$ (α and β refer to the space indices, $\langle \cdot \rangle$ to the thermal noise averaging).

- **DPD** for a set of particles indexed with $1 \leq i \leq N$, with positions $\boldsymbol{r}_i$ and momenta $\boldsymbol{p}_i$ (DPD is not meaningful if one considers only one particle at a time)

$$\dot{\boldsymbol{r}}_i = \frac{\boldsymbol{p}_i}{m}; \tag{3.2}$$

$$\dot{\boldsymbol{p}}_i = \boldsymbol{f}_i(\{\boldsymbol{r}\}) + \sum_{j,(j\neq i)} -\gamma w(r_{ij})^2 \boldsymbol{e}_{ij} \cdot (\boldsymbol{p}_i - \boldsymbol{p}_j)\, \boldsymbol{e}_{ij} + \sum_{j,(j\neq i)} \sigma w(r_{ij}) \boldsymbol{e}_{ij} \psi_{ij}(t). \tag{3.3}$$

  Each particle i exchanges randomly some momentum with a selected set of neighbors j. This exchange dynamics depends on an arbitrary short range function $w(r_{ij})$ and acts along the separation $\boldsymbol{r}_j - \boldsymbol{r}_i$, where $\boldsymbol{r}_{ij}$ stands for $\boldsymbol{r}_j - \boldsymbol{r}_i$, r_{ij} for $||\boldsymbol{r}_{ij}||$ and the unit vector $\boldsymbol{e}_{ij}$ for $\boldsymbol{r}_{ij}/r_{ij}$. To each pair of particles is associated a random noise $\psi_{ij}(t)$, even though only a fraction of the pairs are truly interacting together at a time, due to the finite range of $w(r)$. The prefactor σ must be chosen equal to $\sqrt{2m\gamma k_B T}$, a fluctuation dissipation requirement necessary to ensure the correct thermalization of the system [10].

DPD was later extended to enforce energy conservation, in addition to momentum conservation [11], thus providing the simulated fluid with a proper thermal diffusion coefficient, and paving the way to the study of non equilibrium situations involving thermal gradients. DPD depends on an arbitrary function $w(r)$ which describes the longitudinal friction forces between pairs of particles given their mutual separation r. Some simulations happen to be sensitive to the choice of $w(r)$.

Various discretization schemes have been proposed for integrating both Langevin [12, 13, 14, 15] and DPD [16, 17, 18, 19, 20]. Surprised by an apparent contradiction between two published discretization schemes for the regular Langevin dynamics, [12] and [14], that normally aimed at the same accuracy, we decided to investigate further the Trotter-Strang splitting procedure applied to stochastic differential equations. This allowed us to understand the difference between the two above mentioned results. We also applied this technique to DPD, and obtained as a result two original discretization schemes, that we compared with other known schemes (fig. 3.1). We finally discussed different choices for the function $w(r)$.

Trotter-Strang splitting

The numerical integration of ordinary differential equations is a well established chapter of numerical analysis, with many different schemes at disposal [21]. As far as Newton molecular dynamics is concerned, the Verlet algorithm (and equivalent formulations) has emerged as one of the favorite [15]. This numerical scheme has several advantages.

- The error on positions and momenta, made when a discrete Verlet dynamics with time step Δt is substituted for the exact continuous time motion equation, is of order $\mathcal{O}(\Delta t^3)$. The Verlet scheme is said to be of order two in time.
- The scheme is exactly time reversible when no external force field is acting. It is said to preserve the symplectic nature of the underlying Hamiltonian dynamics, and in particular, the Liouville measure in phase space.

The Verlet scheme can be viewed as the result of a Trotter-Strang splitting of a time evolution operator in phase space (detailed calculations are provided in our manuscript [22]). Any phase space density $\rho(\boldsymbol{r}_i, \boldsymbol{p}_i)$ subject to Hamiltonian dynamics obeys

$$\frac{\partial \rho}{\partial t} = -\hat{\mathcal{L}}\rho = -\sum_i^N \left(\boldsymbol{p}_i \cdot \frac{\partial}{\partial \boldsymbol{r}_i} + \boldsymbol{f}(\boldsymbol{r}_i) \cdot \frac{\partial}{\partial \boldsymbol{p}_i} \right) \rho, \tag{3.4}$$

with $\hat{\mathcal{L}}$ = the Liouvillian operator. Integrations of Newton equations amounts to knowing $\exp(-\hat{\mathcal{L}}t) = \exp(-\hat{\mathcal{L}}\Delta t)^N$, where $N = t/\Delta t$ stands for a number of discrete time steps. The numerical scheme results

from the following approximation of the evolution operator $\exp(-\hat{\mathcal{L}}\Delta t)$:

$$\exp(-\Delta t\hat{\mathcal{L}}) \simeq \exp\left(-\frac{\Delta t}{2}\sum_i^N \boldsymbol{p}_i\cdot\frac{\partial}{\partial \boldsymbol{r}_i}\right)\exp\left(-\Delta t\sum_i^N \boldsymbol{f}_i(\boldsymbol{r}_i)\cdot\frac{\partial}{\partial \boldsymbol{p}_i}\right)\exp\left(-\frac{\Delta t}{2}\sum_i^N \boldsymbol{p}_i\cdot\frac{\partial}{\partial \boldsymbol{r}_i}\right) \quad (3.5)$$

exact up to order Δt^2. The approximation comes from a decomposition of $\hat{\mathcal{L}}$ as a sum of two terms $A+B$, where A contains the derivatives with respect to $\boldsymbol{r}$ and B the derivatives with respect to $\boldsymbol{p}$. The operators A and B do not commute, but one can write $e^{A+B} = e^{A/2}e^B e^{A/2} + \mathcal{O}(\Delta t^3)$. Each one of the exponential terms appearing in eq. (3.5) has the effect of updating momenta without altering positions, or updating positions at fixed momenta, in a well defined order, leading to the following numerical scheme:

$$\boldsymbol{p}_i(t+\Delta t) = \boldsymbol{p}_i(t) + \boldsymbol{f}_i\left(\boldsymbol{r}_i(t) + \boldsymbol{p}_i(t)\frac{\Delta t}{2m}\right)\Delta t; \quad (3.6)$$

$$\boldsymbol{r}_i(t+\Delta t) = \boldsymbol{r}_i(t) + \left(\boldsymbol{p}_i(t) + \boldsymbol{p}_i(t+\Delta t)\right)\frac{\Delta t}{2m}. \quad (3.7)$$

The resulting discretization scheme is equivalent to a Verlet algorithm [15, 8].

Discretization of Langevin equations

Are Langevin equations amenable to similar treatment ? Unlike ordinary differential equations, there is no unique definition for the accuracy of a discrete stochastic scheme. Let us consider for instance the Brownian diffusion described by eq. (3.1).

A discrete scheme is said to be of **strong order** n if the difference $\langle|X_{num}(t+\tau) - X(t+\tau)|\rangle$ between the numerical approximation $X_{num}(t+\tau)$ and the exact function $X(t+\tau)$ after a finite time interval τ is bounded by $\mathcal{O}(\Delta t)^n$, with same initial conditions $X_{num}(t) = X(t)$, where X represents any position or velocity component of the system. Angle brackets $\langle\cdot\rangle$ represent the average with respect to the noise $\boldsymbol{\psi}$. This scheme is said to of **weak order** m if $|\,\langle X_{num}(t+\tau)\rangle - \langle X(t+\tau)\rangle\,|$ is bounded by $\mathcal{O}(\Delta t)^m$. Strong order, also referred as pathwise convergence, is relevant when the noise function $\psi(t)$ is known, as could be a noisy but deterministic function of the time that is integrated upon. Weak order considers only averaged observables and is relevant in situations where the noise ψ has no physical existence but is used as a convenient intermediate. Langevin molecular dynamics belong to the second category. One finds in ref. [23] a number of discretization schemes associated with general stochastic differential equations.

With the help of Jean Farago, we generalized the Trotter-Strang splitting procedure, starting directly from the Langevin equation. One sees that because $||\int_0^{\Delta t}\mathrm{d}s\boldsymbol{\psi}(s)|| \sim \sqrt{\Delta t}$, a simple Trotter-Strang splitting $e^{A+B} \simeq e^{A/2}e^B e^{A/2}$ is exact only up to order Δt, instead of Δt^2 in the deterministic case.

A strategy that immediately springs to mind is to look for an improved, higher-order decomposition of e^{A+B}, such as $e^{7A/24}e^{2B/3}e^{3A/4}e^{-2B/3}e^{-A/24}e^B$ [24]. Unfortunately, results due to Suzuki [25, 26] assert that any higher-order decomposition involves negative signs in front of either operator A or B. Such negative terms, equivalent to a time reversed evolution, are rather innocuous if applied to hamiltonian systems: one can obtain in that way some very efficient integrators [27, 28]. Negative coefficients, however, are problematic if the dynamics is not reversible, because reversing time in the heat diffusion equation causes a singular behavior.

By analogy with the hamiltonian case, we associate to the Langevin equation a time dependent Liouvillian $\hat{\mathcal{L}}(t)$:

$$\hat{\mathcal{L}}(t) = \frac{\boldsymbol{p}}{m}\cdot\frac{\partial}{\partial \boldsymbol{r}} + (\boldsymbol{f}(\boldsymbol{r}) - \gamma\boldsymbol{p} + \sigma\boldsymbol{\psi}(t))\cdot\frac{\partial}{\partial \boldsymbol{p}}, \quad (3.8)$$

Here, a difficulty originates from the time dependence of the noise term in $\hat{\mathcal{L}}(t)$. The evolution operator takes the form of a chronological, or time-ordered exponential. Then, it requires a Magnus expansion to transform time-ordered exponentials into ordinary exponentials, namely [29]:

$$\mathrm{T}\exp\left(-\int_t^{t+\Delta t}\mathrm{d}s\,\hat{\mathcal{L}}(s)\right) = \exp\left(-\int_t^{t+\Delta t}\mathrm{d}s\,\hat{\mathcal{L}}(s)\right) \times\exp\left(-\frac{1}{2}\int_t^{t+\Delta t}\mathrm{d}s\int_0^s\mathrm{d}u\,[\hat{\mathcal{L}}(u),\hat{\mathcal{L}}(s)]\right). \quad (3.9)$$

Applying this identity to the stochastic Liouvillian operator yields exactly the Ermak and Buckholz (EB) algorithm [12, 15], which is a strong order two discretization. This can be shown by comparing the EB scheme to the so-called order-2 strong Taylor scheme explicitly given in [23]. By contrast, the Ricci and Ciccotti scheme [14] (later corrected by Ciccotti and Vanden-Eijden [30]) and the Verlet scheme using the averaged noise and friction forces over the time interval $[t, t+\Delta t]$ are only strong order one scheme, as they differ from the EB scheme by a random increment of variance Δt^3.

However, it turns out that all these schemes share the same weak order of accuracy. As a conclusion, there is nothing to gain from using the Ermak-Buckholz procedure for sampling Langevin trajectories.

Applications to dissipative particle dynamics

Trotter decomposition was applied to DPD, starting from an equivalent Fokker-Planck formulation of the stochastic dynamics [19, 20]. The Fokker-Planck formulation expresses directly the dynamics in terms of averaged trajectories, and leads to efficient algorithms as far as weak convergence is concerned[1].The tradeoff is to deal with second order differential operators in velocities.

We decided to apply the Trotter decomposition to the stochastic DPD equations. This situation is delicate because the viscous friction between pairs of particles depend on their mutual position. The resulting stochastic equations are subject to nonadditive noise, though the Itô and Stratonovitch interpretations coincide [10]. In order to obtain a weak order two algorithm, we must incorporate double commutator corrections to the Trotter decomposition and the Magnus formula (equation (69) of ref. [22] reprinted page 77).

There is a number of possibilities for splitting the exponential operator $\mathrm{T}\exp(-\int \hat{\mathcal{L}}(s)\mathrm{d}s)$. One of them sees the cancellation of all double commutators appearing in the decomposition, thus leading to a genuine weak order two algorithm reproduced below:

$$\begin{aligned}
\boldsymbol{r}(t+\Delta t) &= \boldsymbol{r}(t) + \frac{\Delta t}{2m}\Big[\boldsymbol{p}(t) + \boldsymbol{p}(t+\Delta t)\Big]; && (3.10)\\
\boldsymbol{p}(t+\Delta t) &= \left[\mathbf{1} - \Delta t\,\boldsymbol{\Gamma}\left(\boldsymbol{r}(t) + \frac{\Delta t}{2m}\boldsymbol{p}(t)\right) + \frac{\Delta t^2}{2}\boldsymbol{\Gamma}^2\left(\boldsymbol{r}(t) + \frac{\Delta t}{2m}\boldsymbol{p}(t)\right)\right]\cdot \boldsymbol{p}(t)\\
&\quad + \Delta t\left[\mathbf{1} - \frac{\Delta t}{2}\boldsymbol{\Gamma}\left(\boldsymbol{r}(t) + \frac{\Delta t}{2m}\boldsymbol{p}(t)\right)\right]\cdot \boldsymbol{K}\left(\boldsymbol{r}(t) + \frac{\Delta t}{2m}\boldsymbol{p}(t); t\right), && (3.11)
\end{aligned}$$

where $\boldsymbol{\Gamma}(\boldsymbol{r})$ and $\boldsymbol{K}(\boldsymbol{r})$ are the viscous frictions and forces field in vector form.

Testing DPD algorithms

It is common to perform assays of DPD algorithms with non interacting (perfect) gases. This probes the capacity of the algorithm to establish a Maxwellian distribution of velocities, and deviation from a featureless pair correlation function $g(r) = 1$ signals imperfections with the discretization scheme.

The efficiency of an algorithm depends on both the discretization scheme and the space dependent dissipation $w(r)$. The most usual w is a piecewise linear function of r, such as w_1, simple enough for computational efficiency purpose.

$$\begin{aligned}
w_1(r) &= \left(1 - \frac{r}{r_0}\right), \text{ if } r < r_0;\\
w_1(r) &= 0, \text{ if } r \geq r_0. && (3.12)
\end{aligned}$$

Let us imagine now two non interacting particles colliding face to face with relative velocity v_0. The friction force vanishes when the pair passes at close distance. This singular behavior is likely to be the reason for the artifacts observed in the noninteracting fluid case. We tried a smoother function $w_2(r)$

$$\begin{aligned}
w_2(r) &= \frac{r}{r_0}\left(1 - \frac{r}{r_0}\right) \text{ if } r < r_0;\\
w_2(r) &= 0 \text{ if } r \geq r_0. && (3.13)
\end{aligned}$$

and found that the artifacts were strongly reduced, as expected.

[1] as a by product the Ermak-Buckholz scheme cannot be obtained in this way

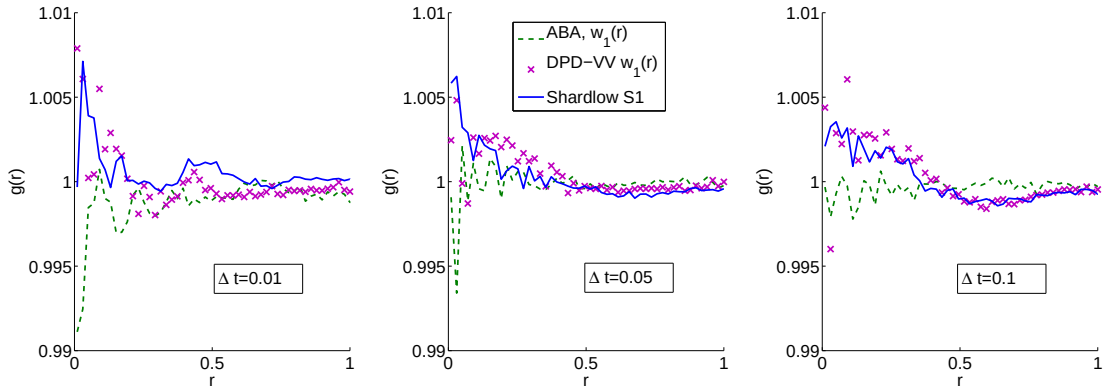

Figure 3.1: Comparison between our algorithm (dashed line ABA) and two other published DPD algorithms [22]. Our algorithm performs fairly well.

3.2 Algorithms for molecular dynamics with non conserved number of particles

F. Thalmann and N.-K. Lee
Fast algorithms for classical $X \longrightarrow 0$ diffusion-reaction processes
Journal of Chemical Physics 130, 074102 (2009), reprinted page 99.

Abstract: The Doi formalism treats a reaction-diffusion process as a quantum many-body problem. We use this second quantized formulation as a starting point to derive a numerical scheme for simulating $X \longrightarrow 0$ reaction-diffusion processes, following a well-established time discretization procedure. In the case of a reaction zone localized in the configuration space, this formulation provides also a systematic way of designing an optimized, multiple time step algorithm, spending most of the computation time to sample the configurations where the reaction is likely to occur.

Algebraic formulation of the Brownian capture problem

We have seen that the Trotter decomposition gives powerful insights on the derivation of numerical discretization schemes. I found the opportunity to use this technique once more in the context of the Brownian capture kinetics (see section 4.1, page 23). More generally, I wanted to treat with this technique situations involving Poissonian changes of discrete state variables. The Doi formalism for Brownian diffusion reaction processes provides the indispensable algebraic operator onto which the Trotter scheme can be used [31, 32, 33].

The Doi formalism recasts the Brownian reaction-diffusion problem

$$\partial_t n(\boldsymbol{r},t) = D\nabla^2 n(\boldsymbol{r},t) - \mu\nabla(n(\boldsymbol{r},t)\boldsymbol{f}(\boldsymbol{r},t)) - S(\boldsymbol{r})n(\boldsymbol{r},t), \tag{3.14}$$

into a second-quantized operator field theory[2]

$$\hat{\mathcal{H}} = \int \mathrm{d}\boldsymbol{r}\Big[D(\nabla a^\dagger(\boldsymbol{r})\cdot\nabla a(\boldsymbol{r})) - \mu(\boldsymbol{f}(\boldsymbol{r})\cdot\nabla a^\dagger(\boldsymbol{r}))a(\boldsymbol{r}) + S(\boldsymbol{r})(a^\dagger(\boldsymbol{r})a(\boldsymbol{r}) - a(\boldsymbol{r}))\Big]. \tag{3.15}$$

In the simple process described by eq. (3.14), particles are not created but only annihilated, as a consequence of the term $-S(\boldsymbol{r})n(\boldsymbol{r},t)$ in eq. (3.14). This leads to a simplified version of the formalism, that can be summarized as below:

$$|\Phi(0)\rangle = a^\dagger(\boldsymbol{r}_0)\,|0\rangle\,; \tag{3.16}$$

$$G(\boldsymbol{r},t) = \langle 0|\,a(\boldsymbol{r})e^{-\hat{\mathcal{H}}\,t}\,|\Phi(0)\rangle\,. \tag{3.17}$$

where $G(\boldsymbol{r},t)$ is the probability of observing the diffusing particle at a position $\boldsymbol{r}$ and time t, given that it was at a position $\boldsymbol{r}_0$ at time 0.

Algorithms for non conserved number of particles

The role of the Liouville operator is now played by $\hat{\mathcal{H}} = \hat{\mathcal{H}}_D + \hat{\mathcal{H}}_F + \hat{\mathcal{H}}_R$, where $\hat{\mathcal{H}}_R$ represents the reaction (or annihilation), $\hat{\mathcal{H}}_D$ the pure Brownian (Fokker-Planck-Smoluchowski) diffusion and $\hat{\mathcal{H}}_F$ the Fokker-Planck drift term. None of these three operators are pair-wise commuting. One of the Trotter-Strang splitting procedure of the evolution operator gives:

$$\begin{aligned} e^{-(\hat{\mathcal{H}}_D+\hat{\mathcal{H}}_F+\hat{\mathcal{H}}_R)\,t} &= \left[e^{-(\hat{\mathcal{H}}_D+\hat{\mathcal{H}}_F+\hat{\mathcal{H}}_R)\Delta t}\right]^{t/\Delta t} \\ &\simeq \left[e^{-\frac{\Delta t}{2}\hat{\mathcal{H}}_R}\cdot e^{-\frac{\Delta t}{2}\hat{\mathcal{H}}_F}\cdot e^{-\Delta t\hat{\mathcal{H}}_D}\cdot e^{-\frac{\Delta t}{2}\hat{\mathcal{H}}_F}\cdot e^{-\frac{\Delta t}{2}\hat{\mathcal{H}}_R}\right]^{t/\Delta t}. \end{aligned} \tag{3.18}$$

[2] A functional formulation of this field theory has been formulated by Peliti [34].

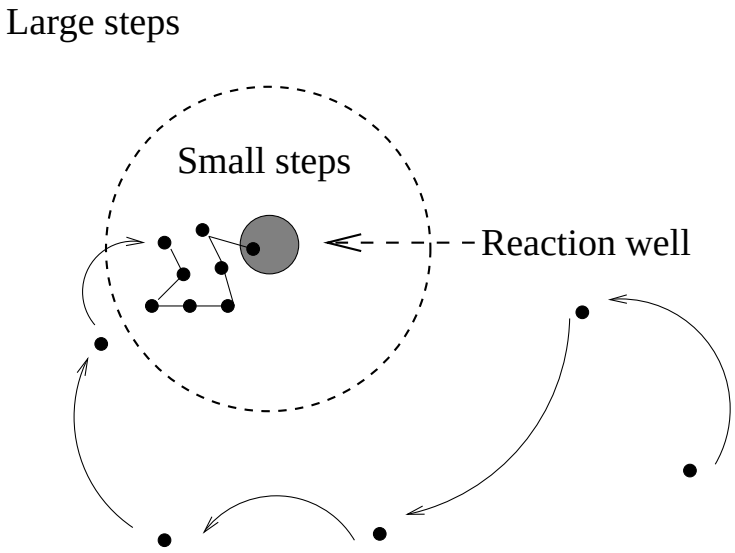

Figure 3.2: Illustration of an variable length step random search of a reaction zone.

One can devise in this way six different splitting schemes, each one of them leading to a different algorithm. The six resulting algorithms shares the same accuracy, and all the resulting terms can be readily interpreted. $\exp(-\Delta t\hat{\mathcal{H}}_D)$ is a simple Brownian diffusion in flat space, $\exp(-\Delta t\hat{\mathcal{H}}_R)$ is a simple decay process and $\exp(-\Delta t\hat{\mathcal{H}}_F)$ is associated with the flow of the ordinary differential equation $\dot{\boldsymbol{r}} = \boldsymbol{f}(\boldsymbol{r}(t))$. The action of the drift operator can be accounted for by any scheme of order 2 for integrating first order autonomous equations, such as the Heun or Collatz schemes [21]. In practice, one substitutes $\tilde{\boldsymbol{f}}(\boldsymbol{r}) = \boldsymbol{f}(\boldsymbol{r} + \Delta t\boldsymbol{f}(\boldsymbol{r})/2)$ for the bare force field $\boldsymbol{f}(\boldsymbol{r})$ to gain one order in accuracy compared with the Euler scheme $\boldsymbol{r}(t + \Delta t) = \boldsymbol{r}(t) + \boldsymbol{f}(\boldsymbol{r}(t))\Delta t$. We obtained as a result the algorithm outlined in Table 3.1.

Multiple time step algorithms

It is very common that the capture region occupies only a tiny part of all accessible configurations. A simple Brownian exploration of the configuration space ends up sampling mostly uninteresting regions far from the capture zone. To improve upon the basic Brownian exploration, one may decide to separate the configuration space into regions that will be sampled with a different characteristic length step (fig. 3.2).

This procedure, however, generates anomalous density distributions of diffusing particles near the boundary between small and large steps regions, due to a local violation of the detailed balance relation. In order to cure this artefact, we suggest to remove the singularity by creating an exchange zone, and by adding an internal state $\sigma = \{A, B\}$ to the diffusing particles. Random switching between state A and B takes place with position dependent rates, so that state A dominates on one side, and B dominates on

Algorithm I: reaction-diffusion over Δt
1. Consider the probability that a particle located at $\boldsymbol{r}(t)$ reacts during a time interval $\Delta t/2$, given that the probability of this event is $1 - \exp(-S(\boldsymbol{r}(t))\Delta t/2)$. If the particle reacts, end the procedure and set the reaction time t_R to $t + \Delta t/2$.
2. Shift the position of the particle by $\mu\tilde{\boldsymbol{f}}(\boldsymbol{r}(t))\Delta t/2$, as a consequence of the drift force.
3. Draw from a Gaussian distribution of variance $2D\Delta t$ a random step $\Delta\boldsymbol{r}^D$, and shift the position by $\Delta\boldsymbol{r}^D$.
4. Shift the position by $\mu\tilde{\boldsymbol{f}}\Big(\boldsymbol{r}(t) + \mu\tilde{\boldsymbol{f}}(\boldsymbol{r}(t))\Delta t/2 + \Delta\boldsymbol{r}^D\Big)\Delta t/2$. The particle sits now at a position $\boldsymbol{r}(t + \Delta t)$
5. Consider the probability that a particle located at $\boldsymbol{r}(t + \Delta t)$ reacts during a time interval $\Delta t/2$. As in step 1, if the reaction takes place, set the reaction time to $t_R = t + \Delta t/2$

Table 3.1: Algorithm for a coordinates dependent $X \to 0$ process

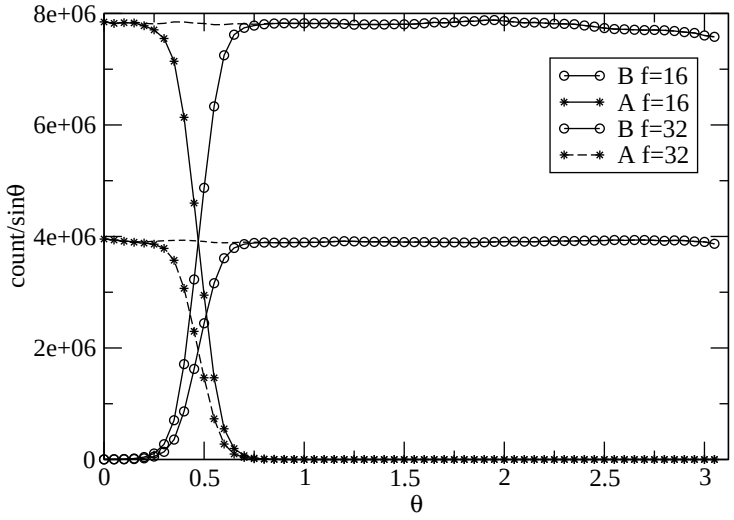

Figure 3.3: Illustration of the exchange zone concept on a sphere. An exchange zone for particle diffusing on a sphere is set up between $\theta = 0.4$ and $\theta = 0.6$, with θ the polar angle. "Slow" A particles are mostly located next to to north pole $\theta = 0$ where the reaction zone is situated, while "fast" B particles are mostly found beyond $\theta = 0.6$. The acceleration ratio between B and A states are respectively $\mathcal{F} = 16$ and $\mathcal{F} = 32$. Nevertheless, the distribution histogram (corrected from its $\sin\theta$ dependence) shows no anomaly around the exchange region.

the other side.

A Doi Hamiltonian $\hat{\mathcal{H}}_\sigma = \hat{\mathcal{H}}_{A,R} + \hat{\mathcal{H}}_{A,D} + \hat{\mathcal{H}}_{A,F} + \hat{\mathcal{H}}_{A,Ex} + \hat{\mathcal{H}}_{B,R} + \hat{\mathcal{H}}_{B,D} + \hat{\mathcal{H}}_{B,F} + \hat{\mathcal{H}}_{B,Ex}$ was introduced to generate the internal state switching, in addition to the diffusion, drift and reaction terms. $\hat{\mathcal{H}}_{A,R}$, $\hat{\mathcal{H}}_{A,D}$,$\hat{\mathcal{H}}_{A,F}$ model respectively the reaction, diffusion and drift of a particle with state A. $\hat{\mathcal{H}}_{B,R}$, $\hat{\mathcal{H}}_{B,D}$,$\hat{\mathcal{H}}_{B,F}$ model the reaction, diffusion and drift of a particle with state B. $\hat{\mathcal{H}}_{A,Ex}$ switches the internal state from A to B and $\hat{\mathcal{H}}_{B,Ex}$ does the opposite. Then a Trotter splitting of the evolution operator (eq. 21 of the manuscript reprinted page 99) leads to a discrete evolution scheme where, while sharing the same underlying dynamics, particles in state A and B evolve with a different time step according to their internal state. We call $\mathcal{F}$ the ratio between the long and the short time steps, typically 8 or 16.

If the $A \leftrightarrow B$ exchange rates are properly chosen, the configuration space splits in two parts, one populated with A particles, the other populated with B particles, with an exchange zone between them in order to remove all artifact relative to the particle spatial distribution. We obtain as a result a multiple time step algorithm with sound foundations.

With the collaboration of N.-K. Lee, we tested this idea with Brownian particles diffusing at the surface of a sphere, with a capture zone located near the north pole, a physical situation described in next Section (fig. 3.3). Numerical simulations durations are cut by a factor which depend on $\mathcal{F}$ and on the respective size ratio between slow and fast domains in configuration space. In the example discussed in fig. (3.3), the exploration of the sphere was roughly six times faster than in the absence of acceleration.

Chapter 4

Colloids

4.1 Capture in rotational colloidal dynamics

N.-K. Lee, A. Johner, F. Thalmann, L. Cohen-Tannoudji, E. Bertrand, J. Beaudry, J. Bibette and C.M. Marques
Ligand-Receptor Interactions in Chains of Colloids: When Reactions Are Limited by Rotational Diffusion
Langmuir 24, p1296-1307 (2008), reprinted page 113.

Abstract: We discuss the theory of ligand receptor reactions between two freely rotating colloids kept at close distance. Such reactions, limited by rotational diffusion, arise in magnetic bead suspensions where the beads are driven into close contact by an applied magnetic field as they align in chain like structures. By a combination of reaction-diffusion theory, numerical simulations and heuristic arguments, we compute the time required for a reaction to occur in a number of experimentally relevant situations. We find in all cases that the time required for a reaction to occur is larger than the characteristic rotation time of the diffusion motion $\tau_{\rm rot}$. When the colloids carry one ligand only and a number n of receptors, we find that the reaction time is, in units of $\tau_{\rm rot}$, a function simply of n and of the the relative surface α occupied by one reaction patch $\alpha = \pi r_C^2/(4\pi r^2)$ where r_C is the ligand receptor capture radius and r the radius of the colloid.

Introduction

The quantitative determination of reaction or association rate coefficients is a major issue in the field of chemical physics. In a certain number of cases, these rates depend on the time it takes for the reactive species to occupy a specific mutual spatial and orientational configuration that enables subsequent association or reaction step. Such rates are said to be limited by diffusion. A particular instance of diffusion limited kinetic coefficient was introduced by Smoluchowski for the bimolecular reaction kinetics of two diffusive spherical reactive species $A + B \rightarrow C$. Smoluchowski found:

$$\frac{\mathrm{d}[A]}{\mathrm{d}t} = -k_{on}[A][B]; \tag{4.1}$$

$$k_{on} = 4\pi(R_A + R_B)(D_A + D_B), \tag{4.2}$$

where R_A and R_B stand for the radii of species A and B, and D_A and D_B are the diffusion coefficients of A and B.

Biochemistry offers numerous examples of multimolecular association (formation of large long-lived complexes) where the mutual diffusion movement of the intervening species is expected to be a key factor controlling the association dynamics. Moreover, the assumption of viscous hydrodynamics is reasonable for large molecules. The Smoluchowski approach was subsequently refined to accommodate various important effects, such as long range forces, strong orientation dependence or hydrodynamic lubrication effects [35, 36]. A remarkable consequence of expression (4.2) is that the association kinetics between pairs of molecules of similar size $R_A \sim R_B$ becomes size independent as $D \sim 1/R$.

According to Bongrand, experimental data sets on antigen-antibody association comfort this observation, showing quite similar association rates but widespread dissociation rates[1],and suggest that diffusion-limited interactions are common in biochemistry (see *e.g.* [36] and references therein)

The relative simplicity of the association kinetics in homogeneous solutions is lost when one of the reactive species is immobilized near a surface, and deriving the correct association rate in this situation is a challenging issue, even though the volumic k_{on} kinetic coefficient is known. Bibette *et al.* found a remarkable application of their superparamagnetic colloidal systems for studying the specific adhesion induced by ligand-receptors pairs bounded to surfaces [37, 38]. In addition to its potential interest for biochemical assays (immunodetection), this method paves to way to a quantitative determination of the association kinetics of constrained ligands and receptors.

Superparamagnetic colloidal beads align as chains under an externally applied magnetic induction field. The chains dissociate when the field is switched off (absence of magnetic remanence) . The average separation between neighboring beads can be adjusted by tuning the magnitude of the induction, balancing between short range repulsion (electrostatic, polymer coating) and dipolar attraction (fig. 4.1). Beads are prepared in order to present a few ligand or receptors at their surface [38]. No association can take place in the absence of magnetic field, when beads are dispersed and remain at some distance. Beads are close enough to promote specific adhesion only when some field is applied, offering an efficient control of the reaction time. The formation of bead doublets can be monitored optically, giving an experimental determination of the advancement of the reaction.

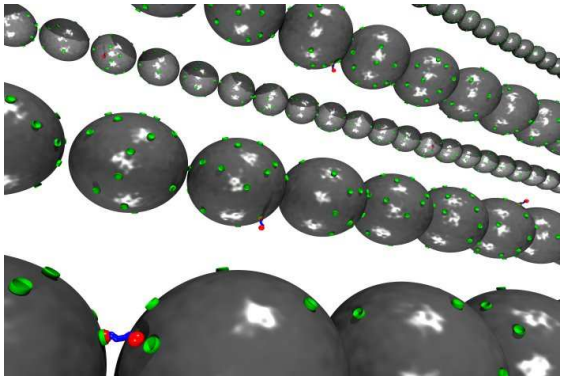

Figure 4.1: Alignment of superparamagnetic beads, with ligand or receptors grafted on their surface (Povray picture by C.M. Marques).

In the article presented here, reprinted page 113, the specific interaction between ligand and receptor is modelled as a *sticking cone* (see figs. 4.2 and 4.3). The rapid variation of the relative separation distance between beads is neglected, and the association problem reduces to the relative diffusion-reaction of Brownian walkers diffusing at the surface of a sphere. Two limiting cases are found:

1/ A single ligand vs a surface fully covered with receptors.

The association takes place as soon as the angle between the ligand and the vector joining the two bead centers becomes less than a critical value θ_C. The irreversible association, or *capture*, between the ligand and any one of the receptors on the opposing surface, is equivalent to a diffusion problem with absorbing boundary conditions (fig. 4.2). The Brownian walker disappears as soon as it crosses the boundary of the capture zone, here a disk parameterized by $\theta = \theta_C$. This approach simply generalizes the Smoluchowski result to a spherical geometry. Absorbing boundary conditions act as weighing with a vanishing coefficient all random trajectories crossing the boundary of the capture zone at least once. An analytical solution is available in this situation.

2/ A single ligand and a single receptor

The problem is formally equivalent to a point diffusing in a curved space $S^2 \times S^2$ reacting with rate

[1]The reported values are 8.0×10^6 $\text{M}^{-1}\text{s}^{-1} \leq k_{\text{on}} \leq 1.8 \times 10^8$ $\text{M}^{-1}\text{s}^{-1}$, compared with 3.4×10^{-4} $\text{M}^{-1}\text{s}^{-1} \leq k_{\text{off}} \leq 6000$ $\text{M}^{-1}\text{s}^{-1}$ [36]

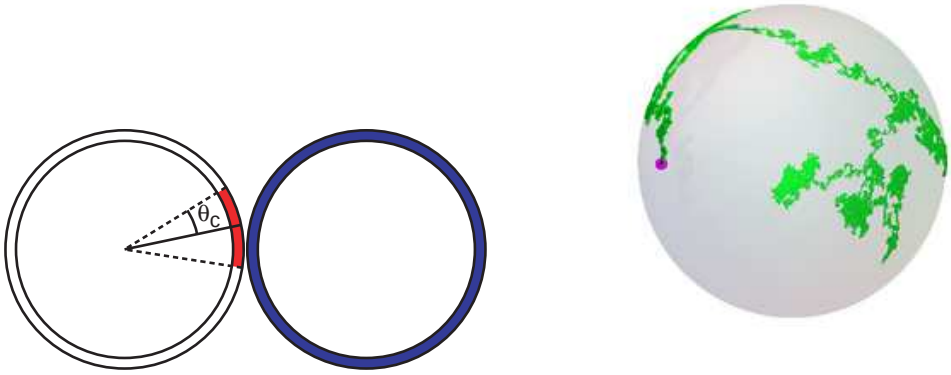

Figure 4.2: The asymmetric case of one ligand *vs* many receptors (left) reduces to a Brownian walker onto a sphere, reacting on the boundary of a small reaction disk, shown in red (right).

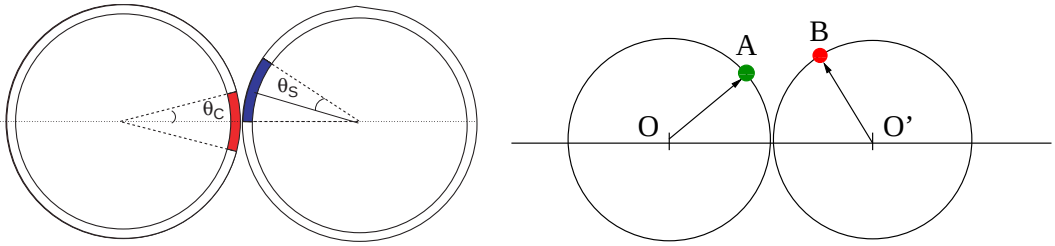

Figure 4.3: Schematic illustration of a single ligand *vs* a single receptor.

q in a reaction zone defined by $\cos(\overrightarrow{OA}, \overrightarrow{OO'}) \geq \cos(\theta_C)$ and $\cos(\overrightarrow{O'B}, \overrightarrow{O'O}) \geq \cos(\theta_S)$ (see fig. 4.3 right). An approximated but accurate calculation can be done using the Wilemski-Fixman-deGennes formulation (WFdG) of reaction-diffusion dynamics [39, 40, 41]. The WFdG formalism expresses the survival probability $\Phi(t)$ in terms of free diffusion propagator (Green function) in configuration space. It provides an accurate approximation to the first passage distribution across the reaction zone when the limit of fast reaction rates $q \to \infty$ is considered, and a rather simple expression for the Laplace transform $\tilde{\Phi}(s)$ of $\Phi(t)$ can then be obtained. In our case, it relates $G_0(\theta, t)$, probability that a Brownian particle diffuses over an angle θ after a time t, to the survival probability $\Phi(t)$. The effective reaction rate, $-\mathrm{d}\Phi(t)/\mathrm{d}t$, follows and depends on time for non exponential relaxations. The main approximation in the WFdG approach consists in factorizing two-point correlation functions into products of two single point correlation functions, which is justified except during a very short transient regime extending over θ_C^2/D.

Capture times

The average capture time τ_C can be expressed in terms of a characteristic Brownian rotation time τ_{rot} and a dimensionless parameter α, where α is the ratio between the area of the capture zone and the area of the colloid. For a single ligand interacting with a bead fully covered with receptors, the average reaction time is

$$\tau_{C,1,\mathrm{full}} = -\tau_{\mathrm{rot}} \ln(\alpha), \tag{4.3}$$

while for a single ligand and receptor on each side, the reaction time is

$$\tau_{C,1,1} = \tau_{\mathrm{rot}} \frac{2\ln(2)}{\alpha}. \tag{4.4}$$

The logarithmic correction in eq. (4.3) is typical of two-dimensional diffusion processes. This first expression can be understood with qualitative arguments (section 2.4 and appendix D of the reprint page 113) while the same arguments find (4.4) only up to a numerical prefactor. Curvature is found to play only a marginal role for small values of α.

A subtle question concerns the evolution of the capture time $\tau_{C,m,n}$ when beads are covered respectively by m ligand and n receptors. So long as the area of the capture zones remain small compared with the total area of the beads, one expects the following scaling to hold:

$$\tau_{C,m,n} = \frac{\tau_{C,1,1}}{m \cdot n} \tag{4.5}$$

It is not possible to establish this result without further assumptions on the spatial repartition of the capture patches, as these different patches compete and screen each other. Arguments are given that support eq. (4.5). As mentioned in [38], experimental association rates are accounted for by angles θ_C corresponding, for beads of diameter 200 nm, to reaction patches of dimension comprised between 0.7 and 11 Angström, depending on the presence of a spacer or not linking the active sites to the surface of the beads.

4.2 Shear induced separation of superparamagnetic aggregates

C. Mendoza, C.M. Marques and F. Thalmann
Enhanced shear separation of superparamagnetic aggregates, submitted, reprinted page 127.

Abstract: We study the designing principles of the simplest colloidal propeller, an architecture built from four identical spheres that can couple translation with rotation to produce controlled drift motion. By considering superparamagnetic beads, we show that the simultaneous action of a magnetic field and a shear flow leads to the migration of the cluster in the vorticity direction. We investigate the dependence of the migration velocity on the geometrical parameters of the cluster, and find that significant cluster separation can be achieved under the typical operation conditions of microfluidic devices.

Propellers and shear induced separation

Our interest in shear separation of colloidal aggregates originates from discussions on the design of simple propellers working on nanometric scale. The propeller effect consists in rotating at constant angular velocity ω a chiral object around a fixed orientation axis, conventionally named z, causing a neat constant drift velocity v_z along z. The propeller efficiency of an aggregate of size L can be expressed as a dimensionless *pitch* $P_p = 2\pi v_z/(L\omega)$ that, in the Stokes flow approximation, provides a size independent characterization of its ability to couple rotational and translational motions. Colloidal science has made so much progress that one can envision the moment where such propellers of nanometric scale will be available. One can imagine a number of interesting situations based on such objects, from microfluidic applications to collective propelling regimes.

An alternative to sophisticated bottom-up designs consists in randomly assembling small colloidal aggregates, for instance with the help of diffusion limited aggregation processes (DLA), and select the ones with the best hydrodynamic properties. Chirality is the key to obtaining a propeller effect, with opposite shear induced migration associated with aggregates that are mirror images of each other (*enantiomers*). Shear flows, with their intrinsic vorticity, coupled to microfluidic devices appear as good candidates for achieving this *hydrodynamic selection* [42].

Unfortunately, Makino and Doi showed some years ago that shear flows alone could not induce an efficient separation between enantiomers, with migration velocities scaling as the cube of the shear rate [43]. The reason is that the Brownian randomization of the orientation of the aggregates prevents them from migrating. To circumvent this limitation, one must find a way to preorient the aggregates with respect to a predefined axis. External magnetic fields are appealing candidates for this task.

Let us outline the reasoning of Makino and Doi, and assume that a chiral object is submitted only to the action of a linear flow with uniform velocity gradient κ_{ij}. Any spontaneous linear velocity drift $\boldsymbol{v}_i$ must obey the tensorial identity (summation on repeated indices):

$$\boldsymbol{v}_i = L_{ijk} \cdot \kappa_{jk} \tag{4.6}$$

If no external factor breaks the isotropy, the tensor L_{ijk} must be invariant with respect to all space rotations. Any such isotropic tensor is proportional to the Levi-Civita volume form $L_{ijk} = L\varepsilon_{ijk}$. As a result, $\boldsymbol{v}_i$ is proportional to the antisymmetric component of the velocity gradient, *i.e.* the rotation component of the flow. The drift velocity ends up being identical to the one induced by a solid rotation flow. Obviously, no migration is expected to arise in this situation. Makino and Doi conclude that a shear flow alone cannot induce a linear migration of the object.

The only way to obtain a linear migration is to break the isotropy of the system. In the manuscript presented here, we investigate how superparamagnetic colloidal aggregates, in combination with magnetic fields can be subject to such shear separation.

The orientation of superparamagnetic aggregates

Superparamagnetic beads acquire a magnetic momentum in the presence of an applied induction field $\mathbf{B}$. As demonstrated at the end of the Section, the optimal orientation of a rigid cluster of superparamagnetic beads is the one minimizing

$$\mathcal{G}(\{\mathbf{B}\}) \simeq -\frac{N\alpha\mathbf{B}^2}{2} + \sum_{i<j} \frac{\mu_0}{4\pi r_{ij}^3}(\alpha\mathbf{B})^2(1-3\cos^2(\theta_{ij})) \tag{4.7}$$

$$\simeq -N\alpha\mathbf{B}^2/2 + 8\varepsilon\alpha\mathbf{B}^2 \sum_{i<j} \left(\frac{a}{r_{ij}}\right)^3 (1-3\cos^2(\theta_{ij})) \tag{4.8}$$

where $\mathcal{G}(\{\mathbf{B}\})$ is a quadratic form in $\mathbf{B}$, and can be regarded as a sum of magnetic dipole-dipole interactions.

Finding the optimal orientation of the aggregate with respect to the external field reduces to finding the lowest eigenvalue of a quadratic form given by (4.8). If the lowest eigenvalue is non degenerate, there will be an optimal orientation axis of the aggregate aligned with $\mathbf{B}$, and the aggregate will be free to rotate freely around this axis. The aggregate can be flipped up-down without energy change. If the lowest eigenvalue of the aggregate is degenerated, then the magnetic induction alone cannot impose a propeller geometry[2].

As shown in the manuscript, reprinted page 127, the presence of too many internal symmetries rules out the existence of a nondegenerate optimal orientation. Let us assume that such a nondegenerated optimal orientation of $\mathbf{B}$ with respect to the aggregate exists. Then any mirror plane of the aggregate must either contain or be orthogonal to $\mathbf{B}$ and any C_2 axis must be parallel or orthogonal to $\mathbf{B}$. C_n axis and rotation-reflections S_n, $n \geq 3$, must lie parallel to $\mathbf{B}$. These orientation rules apply irrespective of the mass and shape of the aggregate. Therefore, tetrahedric, cubic and icosahedric symmetries are incompatible with magnetic induced preorientation.

A further bit of classification can be achieved if one notices that aggregates must be chiral to exhibit a propeller effect or be sensitive to shear separation. The only group-symmetry classes that allows shear induced separation and propelling are C_1 (no symmetry), C_n and D_n, according to the Schoenflies terminology [44]. As a by-product, aggregates cannot be linear or planar, and require at least four different beads to display any shear separation or propulsion effect.

Hydrodynamics of colloidal clusters

We used the Kirkwood-Riseman approach [45, 46] for deriving the equations of movement induced by the flow around the aggregate. If one introduces collective coordinates Q_α for describing the motion of the aggregate (for instance the position of the geometric center and three Euler angles), the equations take the form:

$$\dot{Q}_\alpha = \sum_{\gamma=1,\ldots 6} \mathbf{h}^{(6)}_{\alpha,\gamma}\mathcal{F}_\gamma + \mathcal{U}_\alpha \tag{4.9}$$

The projected mobility matrix $\mathbf{h}^{(6)}_{\alpha,\gamma}$ is a 6×6 symmetric matrix obtained by restricting the inverse hydrodynamic matrix $\mathbf{H}^{-1}$ to the velocity subspace spanned by the collective coordinates Q_α.

$$\mathbf{h}^{-1}_{\gamma,\alpha} = \sum_{m,n} \left(\frac{\partial \mathbf{R}_m}{\partial Q_\gamma} \,\middle|\, \mathbf{H}^{-1}_{mn} \,\middle|\, \frac{\partial \mathbf{R}_n}{\partial Q_\beta} \right) \tag{4.10}$$

$$\mathbf{h} = \left(\mathbf{h}^{-1}\right)^{-1} \tag{4.11}$$

where $\mathbf{R}_n$ represents the Euclidean position of bead n for a given set of coordinates Q_α. $\mathcal{F}_\gamma$ are the external forces and torques components, obtained from the set of external forces $\mathbf{F}^{(e)}_n$ exerted on each bead n:

$$\mathcal{F}_\alpha = \sum_n \left(\frac{\partial \mathbf{R}_n}{\partial Q_\alpha} \,\middle|\, \mathbf{F}^{(e)}_n \right), \tag{4.12}$$

and $\mathcal{U}_\alpha$ are the generalized components of the streaming flow, derived from the velocity field $\mathbf{u}(\boldsymbol{r})$ that would flow in the absence of aggregate [46].

$$\mathcal{U}_\alpha = \sum_{\gamma=1}^{6} \mathbf{h}_{\alpha,\gamma} \cdot \sum_{mn} \left(\frac{\partial \mathbf{R}_m}{\partial Q_\gamma} \,\middle|\, \mathbf{H}^{-1}_{mn} \,\middle|\, \mathbf{u}(\boldsymbol{R}_n) \right). \tag{4.13}$$

[2]Yet a doubly degenerated lowest eigenvalue may suffice to get around the Doi and Makino limitation by breaking the isotropy of the system, but we did not investigate further this situation

Equations (4.9) can then be integrated for a shear flow $\mathbf{u}(\boldsymbol{r}) = \dot{\gamma} y \boldsymbol{e}_x$ with vorticity perpendicular to the field direction $\mathbf{B} = B\boldsymbol{e}_z$.

Using equations like these, and neglecting thermal Brownian motion, we numerically integrated the motion of the aggregate and computed the associated pitches. Our results are valid in the limit of large Peclet numbers, where $\mathrm{Pe} = \dot{\gamma}\tau_c$, is defined as the product of a characteristic diffusion time τ_c with the shear rate $\dot{\gamma}$.

A model aggregate

We took as an example the simplest chiral structure, made of four beads, illustrated in fig. (4.4). In this configuration, bead 1 and bead 2 at a diameter distance $L = 2a$ define the main axis. The third bead, connected to bead 1 defines a lower arm of length L perpendicular to the main axis, and the fourth bead, connected to bead 2 defines an upper arm of length L, also perpendicular to the main axis. The upper and lower arms are separated by an angle δ. Aggregates with angles δ and $-\delta$ only differ in their chirality, they are enantiomers. We consider L as the characteristic size of the aggregate.

The aggregate belongs to the D_2 symmetry group, with a single C_2 rotation axis. For $0 \leq \delta \leq \delta_c \simeq 66.4°$, the magnetic field lies parallel to the axis C_2, a situation termed Λ configuration. At $\delta = \delta_c$ the lowest eigenvalue of the magnetic energy form is accidentally degenerated, and result in a stability exchange in favor of $\mathbf{B}$ perpendicular to the axis C_2 for $\delta \geq \delta_c$, leading to the Σ configuration. In the Σ configuration, the attitude of the aggregate evolves continuously relative to $\mathbf{B}$, with the aggregate helically wrapped around $\mathbf{B}$.

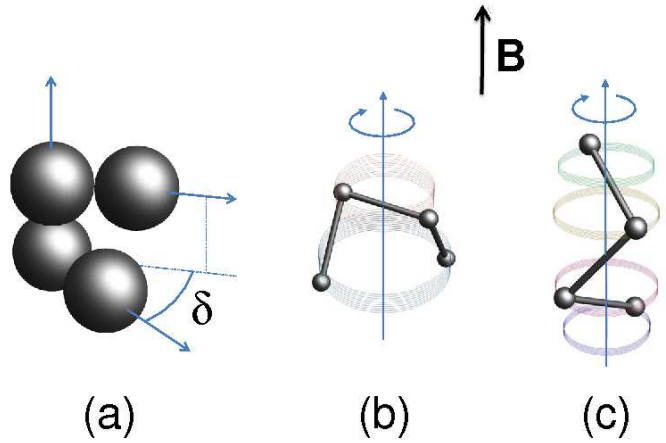

Figure 4.4: Sketch of the colloidal propeller, made of identical superparamagnetic beads. For displaying purposes only, the beads are represented by spheres of a diameter smaller that the arm length in (b) and (c). The propeller consists of a main axis and two perpendicular arms that form an angle δ (a). For small values of δ, one stable equilibrium position under vertical magnetic field, that we name Λ orientation, is shown in (b), the other being obtained by a rotation of 180° around the main axis. For larger values of δ the equilibrium position that we name Σ orientation is shown in (c).

We estimate in the manuscript the magnitude of both propelling (P_p) and shear separation (P_s) efficiencies as a function of the angle δ. Our results are summarized in fig. (4.2), valid in the limit of large Peclet numbers. It is quite surprising to observe that propelling and shear induced migration, while associated with the same angular velocity, takes place in opposite direction in the "Σ" orientation. The drift velocity change its sign twice, and the pitches P_p and P_s seem to vanish simultaneously in fig. (4.2). We therefore demonstrated that shear induced and propeller pitches are related but distinct attributes of the aggregates.

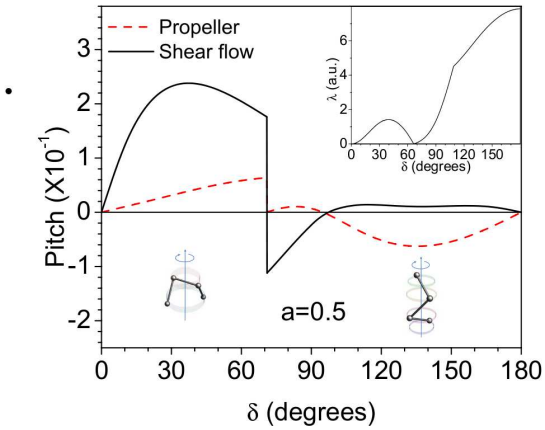

Figure 4.5: Pitches P_s (shear flow, full black line) and P_p (propeller, dashed red curve) as a function of the angle δ for touching beads $L = 2a$. Λ and Σ orientations are depicted on the graph, separated by a critical value δ_c. Inset: stability λ_g of the magnetically oriented aggregate.

Note: derivation of the dipolar magnetic energy

The set of magnetizations $\mathbf{m}_i$ that beads acquire if exposed to an arbitrary inhomogeneous field $\mathbf{B}_i$ can be computed self-consistently. Each magnetic moment $\mathbf{m}_i$ located at M_i creates at M_j a magnetic field:

$$\frac{\mu_0}{4\pi r_{ij}^3}\left(3(\mathbf{m}_i\cdot\hat{\boldsymbol{r}}_{ij})\hat{\boldsymbol{r}}_{ij}-\mathbf{m}_i\right)=\frac{\mu_0}{4\pi r_{ij}^3}\left(3\hat{\boldsymbol{r}}_{ij}\otimes\hat{\boldsymbol{r}}_{ij}-\mathbf{1}\right)\cdot\mathbf{m}_j \tag{4.14}$$

where $r=||\overrightarrow{M_iM_j}||$ and $\hat{r}=\overrightarrow{M_1M_2}/r$. Each bead i experiences a local field due to $\mathbf{B}_i$ and the sum of direct interactions at M_i caused by the magnetic moments $\mathbf{m}_j$.

$$\mathbf{B}_i^{(loc)}=\mathbf{B}_i+\sum_{j\neq i}\frac{\mu_0}{4\pi r_{ij}^3}(3\hat{\boldsymbol{r}}_{ij}\hat{\boldsymbol{r}}_{ij}-\mathbf{1})\mathbf{m}_j \tag{4.15}$$

In the linear regime $\mathbf{m}_i=\alpha_i\mathbf{B}_i^{(loc)}$

$$\mathbf{m}_i+\alpha_i\sum_{j\neq i}\frac{\mu_0}{4\pi r_{ij}^3}(\mathbf{1}-3\hat{\boldsymbol{r}}_{ij}\hat{\boldsymbol{r}}_{ij})\mathbf{m}_j=\alpha_i\mathbf{B}_i \tag{4.16}$$

which can be rewritten as:

$$\frac{\mathbf{m}_i}{\alpha_i}+\sum_{j\neq i}\frac{\mu_0}{4\pi r_{ij}^3}(\mathbf{1}-3\hat{\boldsymbol{r}}_{ij}\hat{\boldsymbol{r}}_{ij})\mathbf{m}_j=\mathbf{B}_i \tag{4.17}$$

and the polarizability tensor reads

$$\mathbf{B}_i = \sum_{j=1}^{n}\left(\frac{\delta_{ij}}{\alpha_i}+(1-\delta_{ij})\frac{\mu_0}{4\pi r_{ij}^3}(\mathbf{1}-3\hat{\boldsymbol{r}}_{ij}\hat{\boldsymbol{r}}_{ij})\right)\mathbf{m}_j \tag{4.18}$$

$$\mathbf{m}_i = \sum_{j=1}^{n}\mathbf{P}_{ij}^{(1)}\cdot\mathbf{B}_j \tag{4.19}$$

$$\begin{aligned}\mathbf{P}_{ij}^{(1)} &= \left[\frac{\boldsymbol{\delta}_{ij}}{\alpha_i}+(1-\delta_{ij})\frac{\mu_0}{4\pi r_{ij}^3}(\mathbf{1}-3\hat{\boldsymbol{r}}_{ij}\hat{\boldsymbol{r}}_{ij})\right]^{-1}_{ij}\\ &\simeq \alpha_i\boldsymbol{\delta}_{ij}+(1-\delta_{ij})\frac{\mu_0\alpha_i\alpha_j}{4\pi r_{ji}^3}(3\boldsymbol{r}_{ij}\boldsymbol{r}_{ij}-\mathbf{1})\end{aligned} \tag{4.20}$$

Remembering that α goes like the volume of a bead, the off-diagonal terms scale like $(d/r_{ij})^3$. Assuming that all beads share roughly the same polarization coefficient α, one realizes that **the parameter ε leading the multipolar expansion** is:

$$\varepsilon=\frac{\mu_0\alpha}{4\pi r_{ij}^3} \tag{4.21}$$

Introducing a "Landau" free-energy depending on magnetizations, the magnetic equilibrium reads:

$$\frac{\partial\mathcal{F}}{\partial\mathbf{m}_i}=\mathbf{B}_i \tag{4.22}$$

leading to the following identification, consistent with a linear polarisability

$$\frac{\partial^2\mathcal{F}}{\partial\mathbf{m}_i\partial\mathbf{m}_j}=[\mathbf{P}]^{-1}_{ij} \tag{4.23}$$

The "Landau functional" reduces to a quadratic form given by the polarization tensor $\mathbf{P}$. Now if the external currents inducing the magnetic field are kept constant, the right thermodynamic potential to consider is not $\mathcal{F}$ but

$$\mathcal{G}(\{\mathbf{B}_j\})=\mathcal{F}(\{\mathbf{m}_i\})-\sum_{i=1}^{n}\mathbf{m}_i\cdot\mathbf{B}_i \tag{4.24}$$

and variations of $\mathcal{G}$ with respect to virtual moves of the aggregate will give us forces, torques, etc. In other words, when one rotates or translates the colloid aggregate at fixed external inducing currents, the magnetic moments $\mathbf{m}_i$ are expected to change. In the case of expression (4.23), this gives

$$\mathcal{G}(\mathbf{B}_j) = -\frac{1}{2}\sum_{i,j}[P^{(1)}]_{ij}\mathbf{B}_j\mathbf{B}_i. \tag{4.25}$$

The best orientation of the aggregate is the one that minimizes the above expression. At the first order in ε, $\mathbf{P} \equiv \mathbf{P}^{(1)}$, one can resort to the following expansion:

$$[P^{(1)}] \simeq \alpha_i \boldsymbol{\delta}_{ij} - \alpha_i\alpha_j \frac{\mu_0}{4\pi r_{ij}^3}(\mathbf{1} - 3\hat{\boldsymbol{r}}_{ij}\hat{\boldsymbol{r}}_{ij})(1-\delta_{ij}) \tag{4.26}$$

to find

$$\mathcal{G}(\{\mathbf{B}_j\}) \simeq -\frac{1}{2}\sum_i \alpha_i \mathbf{B}_i^2 - \frac{1}{2}\sum_{i,j}\frac{\mu_0\alpha_i\alpha_j}{4\pi r_{ij}^3}\left[3(\mathbf{B}_i\cdot\hat{\boldsymbol{r}}_{ij})(\mathbf{B}_j\cdot\hat{\boldsymbol{r}}_{ij}) - (\mathbf{B}_i\cdot\mathbf{B}_j)\right]$$

$$\mathcal{G}(\{\mathbf{B}\}) \simeq -\frac{N\alpha\mathbf{B}^2}{2} + \sum_{i<j}\frac{\mu_0}{4\pi r_{ij}^3}(\alpha\mathbf{B})^2(1-3\cos^2(\theta_{ij})) \tag{4.27}$$

$$\simeq -N\alpha\mathbf{B}^2/2 + 8\varepsilon\alpha\mathbf{B}^2\sum_{i<j}\left(\frac{a}{r_{ij}}\right)^3(1-3\cos^2(\theta_{ij})) \tag{4.28}$$

As the first term does not depend on the orientation of the colloid, only the second term contributes and reduces to a very intuitive expression: the sum of dipolar contributions between beads. The approximation made by using this expression is controlled by ε and is consistent with the use of $\mathbf{P}^{(1)}$.

Chapter 5

Bioinspired Physics

5.1 Dynamical alignment

V.A. Baulin, C.M. Marques, F. Thalmann
Collision induced spatial organization of microtubules Biophysical Chemistry 128, p231-244 (2007), reprinted page 133.

Abstract: The dynamic behavior of microtubules in solution can be strongly modified by interactions with walls or other structures. We examine here a microtubule growth model where the increase in size of the plus-end is perturbed by collisions with other microtubules. We show that such a simple mechanism of constrained growth can induce ordered structures and patterns from an initially isotropic and homogeneous suspension. First, microtubules self-organize locally in randomly oriented domains that grow and compete with each other. By imposing even a weak orientation bias, external forces like gravity or cellular boundaries may bias the domain distribution eventually leading to a macroscopic sample orientation.

A kinetically constrained growth model

The organization and dynamics of microtubules networks is a major domain in biophysics studies. Microtubule cytoskeleton is a key ingredient of cells growth, division and internal trafficking [47]. The interest of Vladimir Baulin in this subject was attracted by a series of publications by J. Tabony *et al.* showing the sensitivity of *in vitro* microtubule network organization to gravity. In particular, in vitro organization of microtubules under microgravity conditions happened to differ significantly from the usual picture, whereas gravity forces do not seem dominant in terms of colloidal organization and reaction rates. His suggestion was to assess whether a kinetically constrained model for microtubule growth could be showing the kind of sensitivity to external perturbations that was necessary to explain the experimental results.

The usual picture of microtubule organization relies on chemical gradients and pattern formation. We numerically and analytically considered a simplified model of microtubule elongation obeying the following kinetic rules in two dimensions.

1. Microtubules depolymerize at their minus end at velocity v_-
2. Microtubules polymerize at their plus end at velocity v_+ if no obstacle is present
3. When a growing microtubule meets an obstacle, *i.e.* another microtubule, the growth stops ("catastrophe"). The microtubule shortens because of its minus end shrinkage.
4. If the obstruction is released, growth resumes ("rescue"). The microtubule length increases as $v_+ > v_-$.
5. Brownian rotational and translational motion is neglected.

Very short microtubules are constantly introduced with random orientation. A given microtubule experiments a sequence of growth and stoppage periods, and disappears from the simulation if shrinkage lasts long enough to reduce its length to zero.

As a result of this kinetically constrained growth protocol, one observes the formation of domains of increasing characteristic size, as depicted in fig. (5.1). The characteristic length eventually increases up to filling the simulation box. The process looks somehow reminiscent from a kinetic domain growth such as those occurring for instance in quenched ferromagnets, excepts that domain boundaries remain sharp, and that the "orientational order parameter" shows no sign of varying smoothly between domains of different orientations. There is nothing like *Néel walls* between the domains, at least in the absence of Brownian agitation.

Once a dominant orientation emerges from the initially random distribution of microtubules, microtubules sharing the dominant orientation see their chances of survival increased and they propagate and reinforce in turn the dominant orientation. This mechanism has been revived in a recent work [48] under the denomination *survival of the aligned*.

We investigated various perturbation to the homogeneous system, such as placing a stationary obstacle in the system, or biasing slightly the initial orientation of microtubule germs. This results in speeding up the orientation of the whole system in a way compatible with the perturbation. This kinetically constrained growth model is thus successful in mimicking the possible role of gravity as the small bias that presides over the global organization of the microtububule network.

Finally we proposed a kinetic model for the distribution of orientation. We found anisotropic solutions, but with domains of finite characteristic sizes. We believe it is difficult to relate our analytical results to numerical simulations because of the strong correlations arising from the low dimensionality of the system, and which are inconsistent with the mean-field assumptions on the collision rates appearing in the analytical model.

Simulations suggest that this mechanism of alignment may work in three dimensional systems either, though its efficiency becomes limited by the diameter of the rods that now plays a role. We finally note that the microtubule bundles appearing in the simulations have no preferential polarization, *i.e.* plus and minus ends of individual microtubules can be found with equal random orientation (blue and red rods on fig. 5.1).

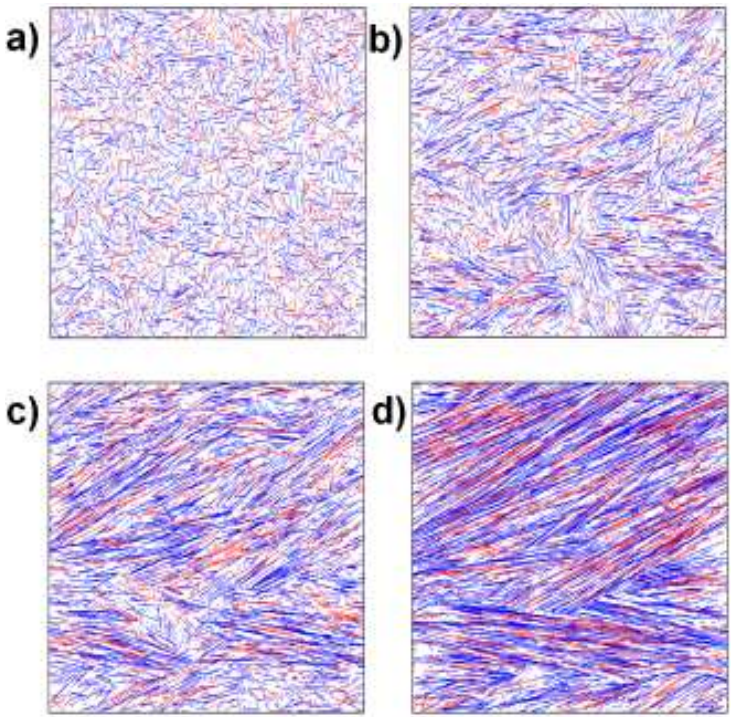

Figure 5.1: Rod orientation with time, induced by the kinetic growth constraint: a mechanism for the alignment of microtubules bundles ?

5.2 Selectivity and molecular recognition

F. Thalmann

A schematic model for molecular affinity and binding with Ising variables European Physical Journal E 31,p441-454 (2010), reprinted page 151.

Abstract: After discussing the relevance of statistical physics in molecular recognition processes, we present a schematic model for ligand-receptor association based on an Ising chain. We discuss the possible behaviors of the affinity when the stiffness of the ligand increases. We also consider the case of flexible receptors. A variety of interesting behaviors is obtained, including some affinity modulation upon bond hardening of softening. The affinity of a ligand for its receptor is shown to depend on the details of their rigidity profile, and we question the possibility of encoding information in the rigidities as well as in the shape. An exhaustive study of the selectivity of patterns with length $n < 8$ is carried on. Connection with other spin models, in particular spin glasses is mentioned in conclusion.

Entropic contributions to shape recognition

The biological world observed at 10 nm scale is radically different from the same reality observed at Angström scale. Enlarging the observation frame by two decades leads to the emergence of radically novel properties associated with macromolecules and macromolecular complexes. In particular, biological macromolecules display specific recognition properties that were absent or hidden on smaller length scales.

The simplest explanation to specific recognition between pairs of complementary molecules is based on shape complementarity, known as the lock and key paradigm of Emil Fischer (see *e.g.* [49]). There is no statistical physics involved at this level of description. On the other hand, one can express the equilibrium association constant of a pair of molecules as a ratio of two properly defined partition functions [50, 36, 51, 52]. It is very satisfactory indeed to know how to express these thermodynamic constants in terms of first principles. The idea behind this work is to investigate, starting from the statistical definition of Gilson *et al.*[50], the binding properties of model flexible objects, and to see how their flexibility can modulate their mutual affinity. Accounting for flexibility amounts to adding internal, or entropic, degrees of freedom to the interacting pair. A number of recent results suggests indeed that entropic contributions [53] and mechanical properties of molecules [54, 55] help tuning the strength of selective interactions between biomolecules.

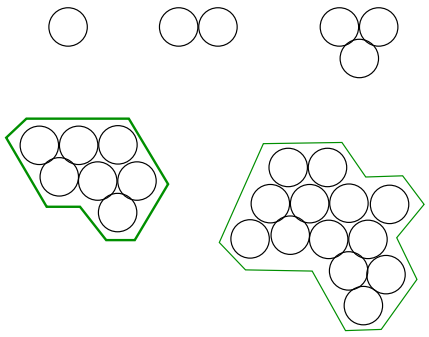

Figure 5.2: Illustration of the emergence of shape coded information when the number of disks forming a 2D aggregate increases.

Equation (5.1) illustrates the statistical formulation of the equilibrium association constant $\mathcal{K}^a_{\mathcal{L},\mathcal{M}}$ for $\mathcal{L}_{\text{free}} + \mathcal{M}_{\text{free}} \leftrightarrow \mathcal{L}\cdot\mathcal{M}_{\text{bound}}$, following Gilson *et al.* [50]. To establish a connection between the microscopic content of the molecules and the macroscopic standard states serving as reference, this expression features the Avogadro number $\mathcal{N}_A$ and the volume per molecule at molar reference concentration V^0, while v stands for the volume accessible to the vector linking the centers of mass of $\mathcal{L}$ and $\mathcal{M}$ in bound state conformation. $Z_{\mathcal{L}\cdot\mathcal{M}\,\text{bound}}$, $Z_{\mathcal{L}\,\text{free}}$ and $Z_{\mathcal{M}\,\text{free}}$ are the respective configurational partition functions of $\mathcal{L}$, $\mathcal{M}$ and $\mathcal{L}\cdot\mathcal{M}$ with fixed center of mass and orientation.

$$\mathcal{K}^a_{\mathcal{L},\mathcal{M}} = \frac{\mathcal{N}_A v}{8\pi^2 V^0} \frac{Z_{\mathcal{L}\cdot\mathcal{M}\,\text{bound}}}{Z_{\mathcal{L}\,\text{free}} Z_{\mathcal{M}\,\text{free}}}. \tag{5.1}$$

$$= \frac{\mathcal{N}_A v}{8\pi^2 V^0} \mathcal{C}^a_{\mathcal{L},\mathcal{M}} \tag{5.2}$$

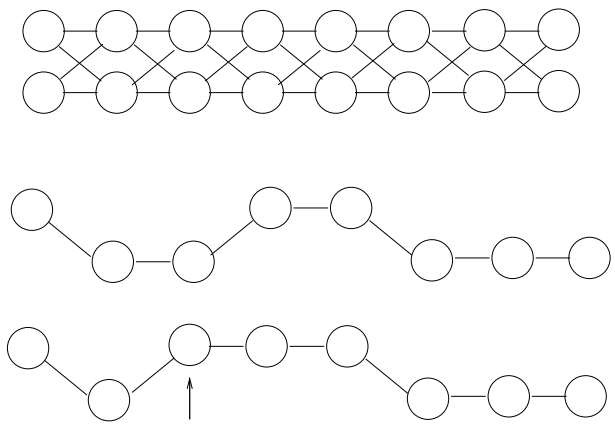

Figure 5.3: Top: set of all possible shapes of our model ligand. Middle: shape described by a spin sequence $s_1 = 1$, $s_2 = -1$, $s_3 = -1$, $s_4 = 1$, $s_5 = 1$, $s_6 = -1$, $s_7 = -1$, $s_8 = -1$. Bottom: new shape obtained by reversing spin s_3. Ground state conformations are enforced by choosing a sequence of ferro and antiferromagnetic next-nearest neighbors couplings. The ligand depicted at the bottom is the ground state shape of $J_{12} = J_{23} = J_{56} = -J$, $J_{34} = J_{45} = J_{67} = J_{78} = J$.

To consider flexibility in ligand receptor association in the simplest way, I introduce a schematic model for pair binding based on Ising chains. As nothing is better known than Ising model physics, the interest of this approach, if any, lies entirely in the interpretation of the results. Note that my approach shares a formal similarity with Ising based description of the hydrophobic-polar model of selective polymer adsorption on surfaces [56, 57, 58].

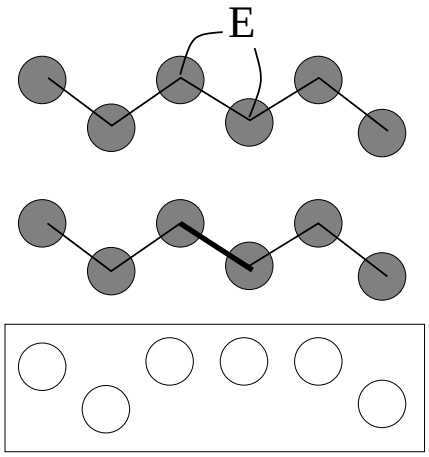

Figure 5.4: Ligand-receptor pair with shape mismatch. The flexible ligand (middle) does not fit in the rigid receptor (bottom). Increasing the third bond stiffness worsens the effect of the mismatch and reduces the affinity of the pair (fig. 5.5). The bond stiffness modulation may be interpreted as a consequence of the presence of an effector molecule (top).

I propose a model where ligand and receptor are treated on the same footing. The conformations of ligand molecules are described with Ising variables s_i while their ground state shape is encoded in the nearest neighbors coupling constants $J_{i,i+1}$ (fig. 5.3). The partition functions Z intervening in the association constant (5.1) are computed exactly by multiplying numerically transfer matrices. Differentiation

with respect to temperature determines the respective energetic ΔU and entropic ΔS contributions to the complex formation free-energy ΔF. Volume changes are neglected so that there is no need to distinguish between Gibbs and Helmholtz free-energies.

In the case of figure 5.4, I investigate the consequence of modulating the stiffness of one specific bond on the thermodynamic stability of the pair. Graph 5.5 shows that the affinity decreases upon hardening this bond. One may speculate on the possibility of modulating in such a way the affinity between two molecules by means of an *effector molecule* that would act as stiffening one region in the ligand.

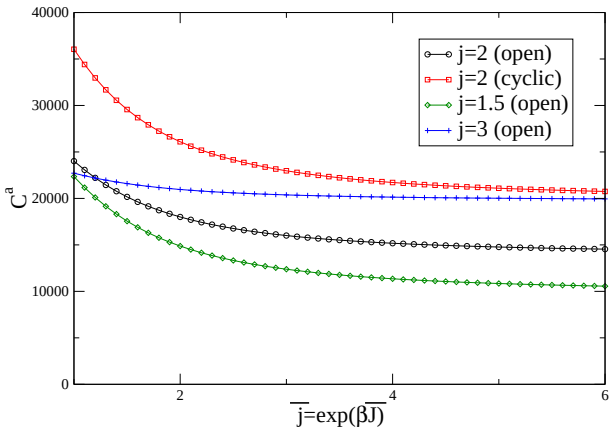

Figure 5.5: Decrease of the affinity of the pair depicted in fig. (5.4). This illustrates how an external effector can alter the mutual affinity of a pair without altering their shapes, a possible entropic allostery mechanism.

Similarly, various interesting behaviors were found, such as nonmonotonic dependences in the affinity constants (see fig. 5.6).

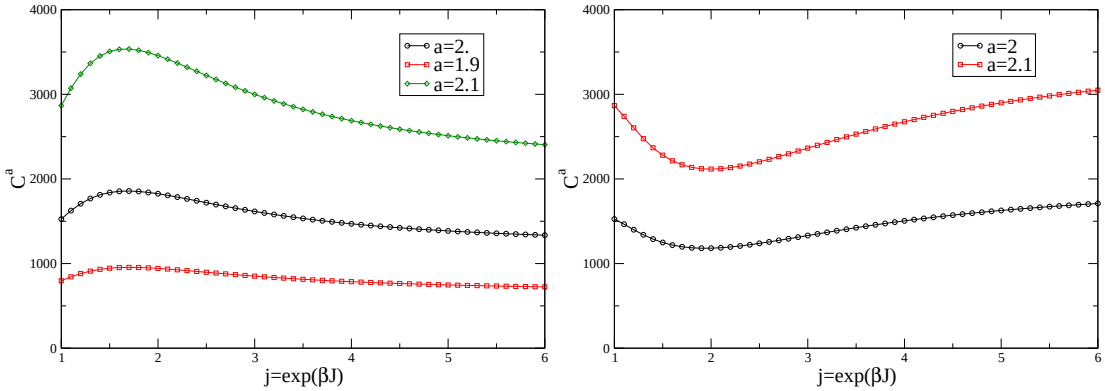

Figure 5.6: Two kinds of nonmonotonic behaviors of the affinity obtained by hardening one specific bond in the pair $\mathcal{L}$-$\mathcal{M}$.

In particular, our model makes it possible to compare pairs of partner molecules with identical shapes but different stiffness profiles. To take an extreme view, one may wonder whether it is possible to induce a specific recognition by acting only on the rigidity pattern, but not altering the shape. As specific recognition and information coding are related, this would be equivalent to store information in stiffness rather than shape patterns. More precisely, one should search for a quadruplet A, B, C, D with identical shape but distinct stiffness profiles, verifying:

$$\begin{aligned} \mathcal{K}^a_{AC} &\sim \mathcal{K}^a_{BD} \\ \mathcal{K}^a_{AC} &\gg \mathcal{K}^a_{AD} \\ \mathcal{K}^a_{BD} &\gg \mathcal{K}^a_{BC} \end{aligned} \tag{5.3}$$

I could not find such pairs of complementary stiffness profiles, and had to satisfy myself with stiffness modulation, but not control, of the affinity.

5.3 On the interactions between membrane and polymer decorated surfaces

F. Thalmann, V. Billot and C.M. Marques

Lipid bilayer adhesion on sparse DNA carpets: theoretical analysis of membrane deformations induced by single end-grafted polymers, submitted, reprinted page 169.

Abstract: We consider a single end-grafted polymer chain covered by a membrane in contact with a flat and rigid surface, in the context of supported membrane adhesion on surfaces carrying dilute polymer brushes. The fluid membrane, adheres to the surface due to non specific attractive interactions. The presence of a macromolecule locally hinders the membrane-surface contact and alters the shape of the membrane. We provide scaling estimates of both size and elevation of the membrane deformation, as a function of curvature modulus, surface tension, adhesion energy and chain gyration radius, leading to various confinement regimes. We also propose a quantitative, self-consistent prediction of the membrane deformation, accurate for shallow bulges. Realistic shapes are computed that could be experimentally observable under weak adhesion conditions.

Adhesion of membranes on dilute DNA carpets

A number of experiments performed in the Membrane and Microforces group (M^3) at the Charles Sadron Institute involve the adhesion of giant vesicles on functionalized surfaces (fig. 5.7), based on the experimental protocol initially developed by T. Gisler at the University of Konstanz [59, 60]. In these experiments, mobile biotinylated binders are incorporated into the phospholipid bilayer of giant unilamellar vesicles (GUV). These molecules bind tightly to streptavidin proteins adsorbed on the surface, forming non-covalent but permanent bonds.

This streptavidin coating is used to end graft to the surface a certain density of double stranded DNA molecules, extracted from the λ-phage viral genome. These DNA molecules are monodisperse chains, with a total of 48502 base pairs. There are a number of fluorescent dyes that specifically bind to the DNA double helix and makes possible a direct imaging of these molecules with conventional or confocal fluorescence microscopy.

The idea behind [59, 60] is to combine a reflection-interference contrast method (RICM) [61] sensitive to the presence of a membrane at the immediate vicinity of the surface, and fluorescence microscopy to study the interaction between a giant vesicle and the DNAs. A number of experiments suggested that in some cases, membranes could form bulges above DNA chains in mushroom conformation, as illustrated in fig. 5.8. These observations prompted our theoretical effort in order to predict the outcome of such interaction in the most general case. Meanwhile, we developed a numerical model for the elevation profile of the membrane above the surface, in order to interpret quantitatively the experimental observations.

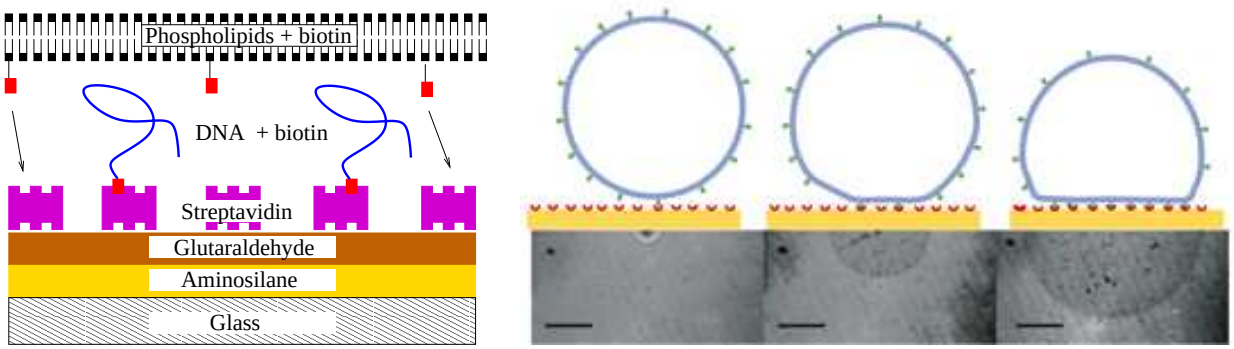

Figure 5.7: Left: principle of the phospholipid membrane functionalization leading to surface adhesion. Right: dual RICM-epifluorescence real time imaging of a GUV adhering on the surface [59]

Scaling predictions

Our membranes are considered as nonfluctuating, infinitely thin bidimensional objects. Their mechanical properties are characterized by two parameters κ and γ. The curvature modulus κ, with the dimension of an energy, controls the Helfrich quadratic curvature contribution [62, 63, 64, 65]. It indicates the energetic cost associated with bending the membrane. The surface tension γ, with the dimension of an energy per area, is related to the energetic cost of increasing the membrane area. In the case of a fluctuating membrane, the concept of surface tension is subtle and depends on the observation scale [66, 67]. Our model membranes have no shear modulus, due to their liquid-crystalline order (in-plane fluidity *vs* out-of-plane elasticity) [68].

We assume that membrane-surface interactions are non-specific and entirely characterized by a single parameter w, with the dimension of an energy per area. This, of course, limits our approach as far as specific adhesion experiments are concerned, but is nevertheless a very instructive preliminary step in view of modeling theoretically adhesion phenomena. Finally, polymer chains are characterized by a Flory radius R_F, and we assume that they interact with both surface and membrane only through steric repulsion. We address the case of ideal Gaussian chains, where R_F reduces to a gyration radius R_G, and self-avoiding chains obeying a Flory scaling. The energy scale of all entropic confinement terms is the thermal one k_BT.

As an illustration of our scaling predictions, I provide below the state diagram of an ideal chain confined by a membrane, with fixed surface tension and temperature, as a function of the curvature modulus κ and the adhesion parameter w (fig. 5.9).

Quantitative prediction of bulge shapes

For comparing our theoretical predictions with experimental results, we developed a self-consistent calculation of the membrane elevation valid for shallow profiles, or bulges. Starting from an initial profile $h_i(r)$, we compute the pressure $p(r)$ exerted on the membrane by a confined Gaussian chain, following [69]. The calculation requires several assumptions: rotation invariance of the profile, Derjaguin approximation with slowly varying $h(r)$, elevation larger than the monomer length scale. Then, we compute the mechanical response of the elastic membrane to the exerted pressure, using an exact response function, which gives in turn a new elevation profile $h_f(r)$. The calculation is repeated until self-consistence. We provide in our manuscript, reprinted page 169, tables of elevation D and radius L of bulges for a wide range of parameters w, κ, γ.

For instance, we applied our method to λ-phage DNA chains, here considered as ideal (though this is not exactly true) with the following characteristic parameters: contour length $L = 20$ μm, persistence length $l_p = 50$ nm, monomer separation $a = 0.3$ nm and gyration radius $R_F = 0.56$ μm [70, 71]. DOPC (dioleoyl-phosphatidylcholine) membranes at room temperature have a measured curvature modulus of about 20 k_BT [59]. Our last parameter, the adhesion coefficient w, has been estimated by Swain and Andelman [72] and ranges between 5.1×10^{-6} J.m^{-2} (strong adhesion, stabilized by hydration forces) and 1.9×10^{-9} J.m^{-2} (weak adhesion, stabilized by Helfrich steric repulsion forces).

For instance, we predict that for $w = 5.1 \times 10^{-6}$ J.m^{-2}, $L \simeq 0.2$ μm and $D \simeq 0.05$ μm. This corresponds to subwavelength bulges. The other limiting case, $w = 1.9 \times 10^{-9}$ J.m^{-2}, leads to stronger deformations of the membranes, namely $L = 3$ μm and $D = 0.5$ μm. It therefore makes sense to search

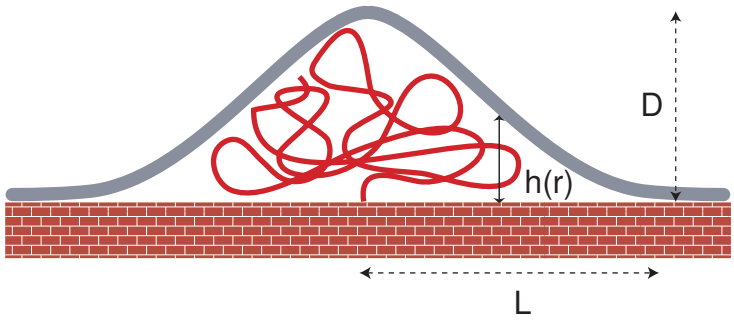

Figure 5.8: Artist view of a semi-flexible chain confined by a membrane in bulge conformation.

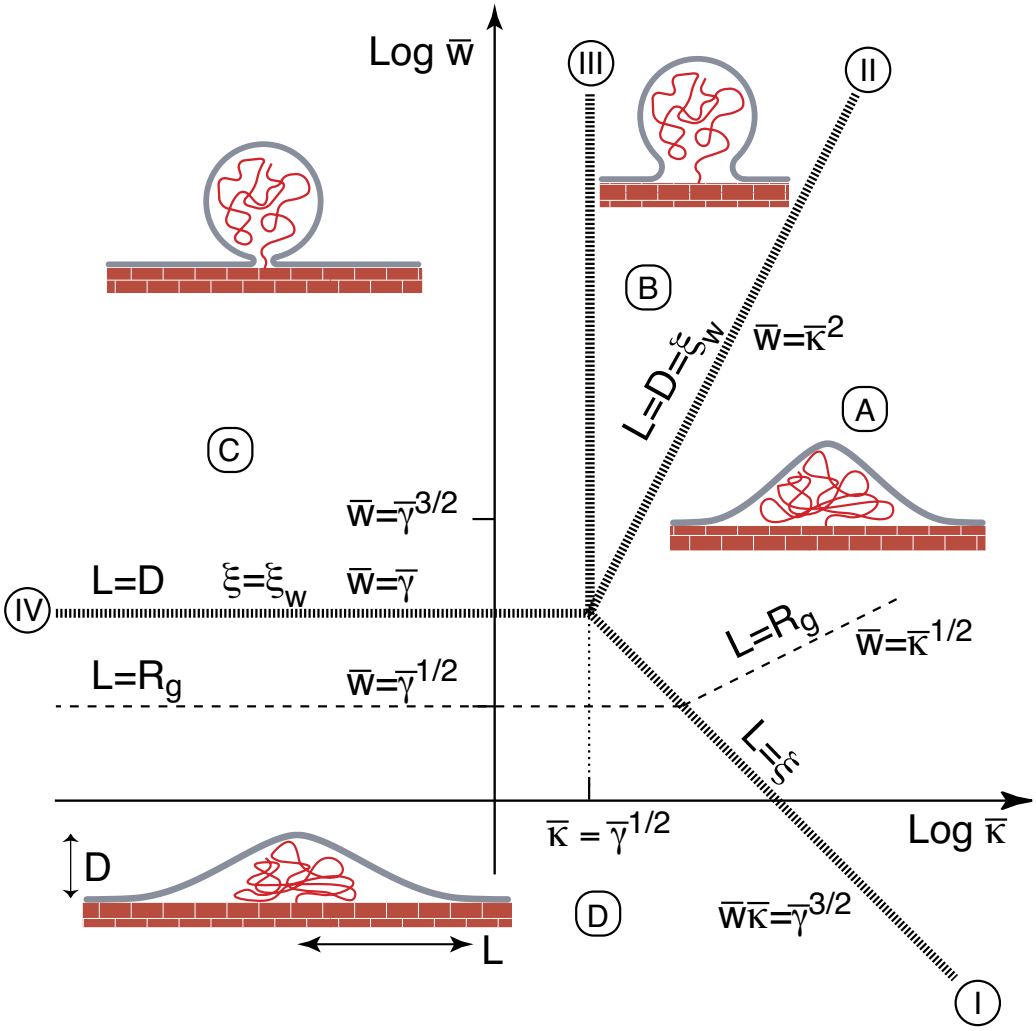

Figure 5.9: State diagram of an ideal chain at fixed gyration radius R_G, temperature T and tension γ, as a function of dimensionless curvature $\overline{\kappa}$ and adhesion $\overline{w}$. Upper left part: balloon shape of the membrane around an unconfined polymer chain with tight neck. Lower left part: bulge shape of the membrane above an unconfined polymer chain. Right part: bulge shape of membrane topping a confined chain. Upper right part: balloon shape of the membrane wrapping a confined chain.

for optical signatures of bulge deformations provided sarfaces are prepared in a way that reduces the interactions with the membrane.

Chapter 6

Perspectives

I list below, for each one of the seven papers or manuscripts presented in the past Sections, what I consider as the most interesting and appealing question or problem to address, echoing the results that have been presented.

6.1 On paper 1, Section 2.1

Brownian hydrodynamics

A natural extension of our work would be to check the result of a Trotter-Strang decomposition on the stochastic evolution of particles subject to hydrodynamic interactions. Let us consider a cloud of small colloidal particles with mass m and position $\boldsymbol{r}_i(t)$ obeying the following set of stochastic equations:

$$m\ddot{\boldsymbol{r}}_j + \sum_{i=1}^{N} \mathbf{H}_{ji}^{-1}(\boldsymbol{r}_k)\dot{\boldsymbol{r}}_i(t) = \boldsymbol{\psi}_j(t) + \boldsymbol{f}_j(\boldsymbol{r}_k) \tag{6.1}$$

where $\mathbf{H}^{-1}$ represents the inverse hydrodynamic tensor, $\boldsymbol{f}_j$ the various force fields and $\boldsymbol{\psi}_j(t)$ the stochastic noise. Thermal equilibrium requires $\langle \boldsymbol{\psi}_i(t)\boldsymbol{\psi}_j(t')\rangle = 2k_BT\delta(t-t')\mathbf{H}_{ij}^{-1}(\boldsymbol{r}_k)$. As for DPD, the dissipation terms depends on position and connects pair of particles. Difficulties arise as one must invert numerically the tensor $\mathbf{H}$, the only one for which an explicit expression is available. Is it possible to obtain in this way a tractable algorithmic formulation of this dynamics ?

Note that long ago, Ermak and McCammon proposed an algorithm for Brownian dynamics simulations involving only positions (the overdamped limit with a vanishing mass in the above equation) which does not requires the numerical inverse of eq. (6.1)[73].

6.2 On paper 2, Section 2.2

Multiple-Time step algorithms

Multiple time step algorithms have been introduced in connection with molecular dynamics of biomolecules (see *e.g.* [74, 75]). The rationale behind these algorithms is to treat slowly varying forces field and rapidly varying force fields on a different footing, updating the former less often than the latter. What we propose instead is to tune the dynamics to the actual configuration of the system. Based on internal state switching, one can devise a number of multiple time step discretization schemes, coupled to deterministic or stochastic motion equations either. It will then be interesting to propose and try to combine a discrete Poissonian internal dynamics with an energy conserving Newtonian molecular dynamics.

Fluorescence transfer

A possible application for the algorithms appearing in paper 2 is mentioned in the last paragraph of my *research project*. It concerns the modeling of the fluorescence emission of probes embedded in phospholipid membranes.

6.3 On paper 3, Section 2.3

As discussed in the previous paragraph, two dimensional reaction diffusion processes appear in various nanoscopic systems.

There is however a nice and appealing generalization of the capture process described in paper 3, which concerns interacting beads. As a matter of fact, lubrication layers and interdigitating polymer brushes between beads should end up correlating the mutual rotation of two neighboring beads. An extreme case is provided by two beads in contact subject to kinetic constraints such as (1) no slip condition, (2) no twist condition (see fig. 6.1). These kinetic constraints are expected to lower the effective dimensionality of the diffusion movement compared with the free case. In particular, in the absence of twist and slip, the configuration space in the single ligand-receptor pair remains four-dimensional while kinetic constraints locally reduces the motion of the representative point in configuration space to two. Therefore, it would not be surprising to recover logarithmic corrective terms typical from two dimensional diffusion in this case also.

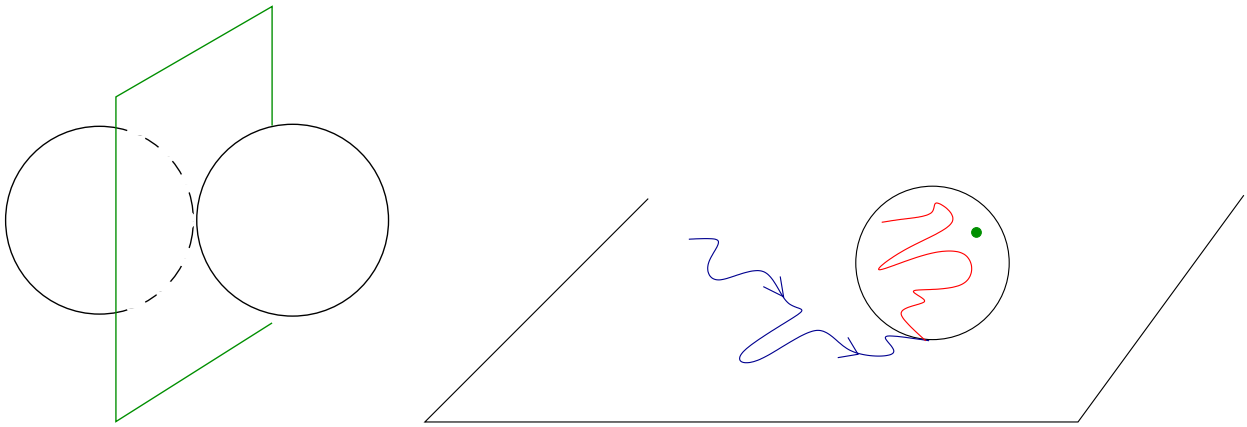

Figure 6.1: Left: two spheres in contact with no slip conditions are found equivalent to a sphere in contact with a planar surface (mediator plane). Right: the Brownian trajectory of the center of mass of a sphere with no slip conditions can be mapped onto the spherical surface, resulting in a well defined spatial orientation of this sphere, see *e.g.* [76]. There is in this case a one-to-one correspondence between the path followed by the center or the sphere and the orientation of the sphere (holonomy).

6.4 On manuscript 4, Section 2.4

A continuation of our investigations relative to physical separation in viscous flows will necessarily involve regimes of intermediate Peclet number. In other words, the inclusion of thermal forces will be required. Such numerical simulations could be implemented along the lines developed in paper 1, with the possibility of benchmarking various algorithms.

The Doi and Makino theorem ruling out linear migration in shear flow can be challenged in a number of ways. For instance, the presence of rectangular wall channels in a microfluidic experiment might have an influence by breaking the rotation invariance that underpins their result. Along the same line, one may conjecture that a lattice of dense, parallel thin wires may also break this rotation invariance (fig. 6.2). Should we then expect a linear migration in that case ?

6.5 On paper 5, Section 2.5

A number of recently published papers explore other aspects of the collisional dynamics ordering of microtubule bundles, and in particular ref. [48, 77]. A very interesting mechanism that these authors add to explain the formation of cortical bundles is a process where a microtubule hitting another microtubule with an acute angle can keep on growing parallel to the obstructing microtubule (while in our case, it always stops). I believe that if we had included such a mechanism, we would have obtained bundles with a coherent, macroscopic orientation.

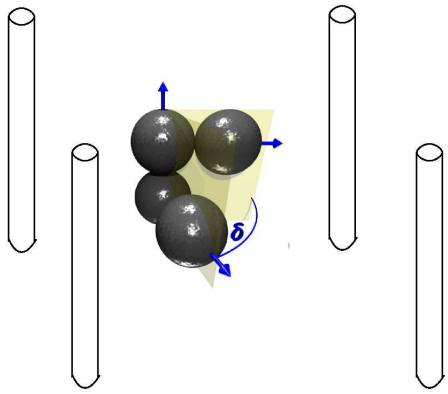

Figure 6.2: An aggregate surrounded by vertical wires and subject to shear flow with vorticity parrallel to the wires could be subject to a linear shear induced vertical migration.

6.6 On paper 6, Section 2.6

Dynamics

I would like to consider a dynamic version of the pair-binding dynamics and to investigate the way flexibility acts on the dynamical association and dissociation constants k_{on} and k_{off}. The current model is simple enough to envision dynamical Monte-Carlo simulations. Considering for instance two ligand-receptor pairs sharing the same equilibrium constant but different stiffness patterns would be quite instructive.

Cooperative binding across a membrane

I am interested in studying cooperative binding effects across a membrane. A special class of molecules is promising for this purpose: the bolaamphiphiles (or bolalipids). Bolaamphiphiles are membrane spanning molecules, either of natural origin[1] or chemically synthesized (see *e.g.* [79]).

Bolaamphiphiles in a spanning conformation connect the two opposite half-spaces separated by the membrane, and can create correlated chemical patterns on the opposite sides of the membrane. A number of ongoing projects, including one conducted in our Institute, aim at designing molecules that can promote a specific and cooperative binding of molecules across a small patch of membrane (see *e.g.* [80]). Cooperative binding means that the probability of having two molecules adsorbed across the same patch of membrane is much higher than having them adsorbed on different portions of the same membrane. The adsorption of one species preorganize a molecular imprint facilitating the subsequent adsorption of the second molecule on the opposite side.

One can easily devise idealized models for describing this situation, using spin variables on a lattice in the presence of quenched random fields that represent the chemical patterns associated with the interacting molecules. These models are nothing but natural extensions (though bidimensional) of the spin model introduced and discussed in paper 6. As a proof, let us consider the following particular case.

We assume that a membrane is composed of 4 different kinds of functionalized bolaamphiphiles, shown in fig. (6.3). These 4 kinds of bolaamphiphile molecules are respectively BB (blue-blue on the figure), RR (red-red), BR (blue-red) and RB (red-blue). The membrane composition is uneven, with concentrations obeying $C_{BB} = C_{RR} \gg C_{RB} = C_{BR}$. When two "molecules" adsorb, bolaamphiphiles are recruited to match the specific patterns of each adsorbed molecule. A positive vertical match (blue-blue or red-red) is associated with a negative favorable energy $-\varepsilon$ while a vertical mismatch (blue-red) is associated by a negative unfavorable energy $+\varepsilon$. We assume no lateral interaction between lipids. As their concentration is lower, the mixed molecules (BR and RB) have a negative chemical potential μ compared with the single color molecules (BB and RR).

A mismatching pattern can be fitted either with a rare BR or RB molecule, or with a common BB or RR molecule, but at some energetic cost $+2\varepsilon$. Summing over the four possible cases, one finds that

[1] they are common in the so-called *extremophile* organisms, such as the *Archae* bacteria found in the hot hydrothermal springs [78]

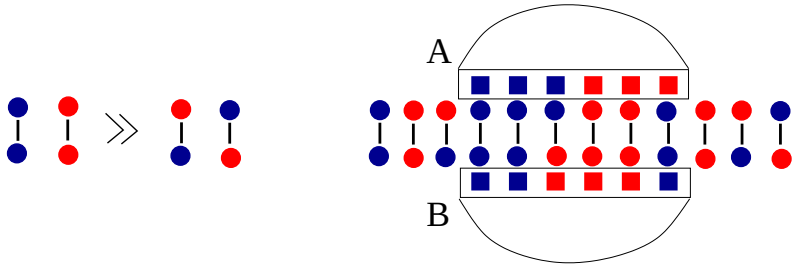

Figure 6.3: Left: four different bolaamphiphile molecules forming a membrane. Right: cooperative binding between two mismatching patterned molecules.

the contribution to the partition function of a matching element is $2\mathrm{ch}(2\varepsilon) + 2\exp(\mu)$, and that the contribution of a mismatching element is $2 + 2\mathrm{ch}(2\varepsilon)\exp(\mu)$. If all four molecules are in equal proportion, $\mu = 0$, and one finds no difference between matching and mismatching patterns. The cooperative binding is not specific nor selective. If, however, the proportion of mixed molecules is scarce, $\mu \ll \varepsilon$. Matching elements become more favorable and there should be a positive bias in favor of the cooperative binding of molecules with matching patterns. This example is a special instance of the schematic model introduced in paper 6, which shows how generic these spin models are as far as selective interactions are concerned.

6.7 On manuscript 7, Section 2.7

The numerical model presented in manuscript 7 can be used for analyzing experimental profiles obtained with a dual RICM-fluorescence microscopy technique (see fig. 6.4). Fig. 6.4 provides an example of comparison between an experimental and a numerical membrane bulge profile, it would be interesting to carry out a systematic study as a function of the different parameters of the system.

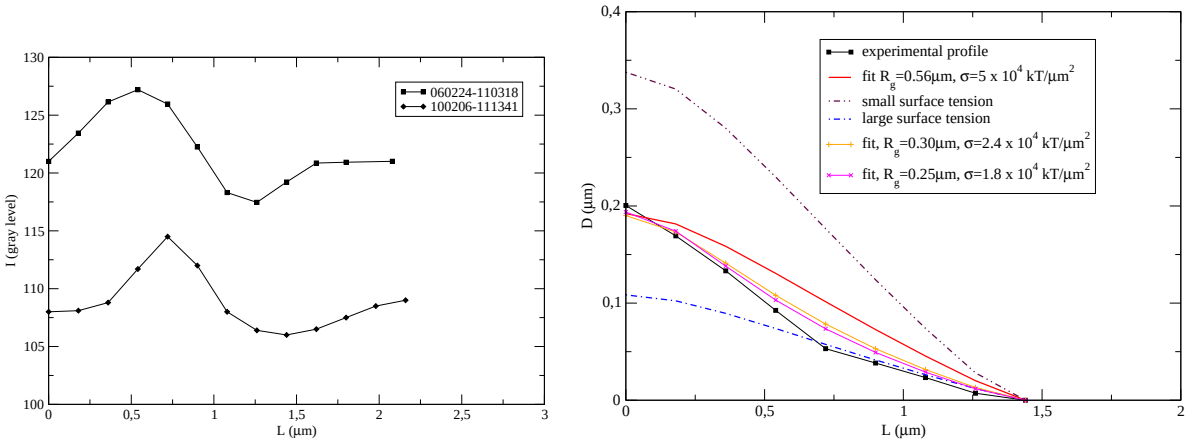

Figure 6.4: Left: grey level intensity profile, obtained using RICM and local averaging of the signal (M.L. Hisette, A. Schroder). Right: Profile reconstruction and comparison with our theoretical model. σ represents the membrane surface tension.

Part II

Research project

Chapter 7

Statistical Physics of Lipid Mixtures and Membrane Dynamics

My research project is two-fold. A first topic concerns phase equilibria in phospholipid mixtures. A second topic extends our previous approaches on the diffusion limited dynamics, with application to the adhesion of membranes and to the diffusion dynamics of fluorescent probes.

7.1 Phase separation in phospholipid bilayers

Phospholipid molecules count among the major constituents of biological membranes. These surfactant molecules spontaneously self-assemble in water solutions to form single or multilamellar phases, with morphologies that lend themselves to experimental control. Giant unilamellar vesicles, for instance, are well appropriate for probing the mechanical and adhesive properties of the membranes.

There is, in the realm of living organisms, an impressive variety of phospholipid molecules with diverse physical and chemical properties. This diversity originates from a modular chemical structure, allowing for many combinations of the hydrophilic and hydrophobic moieties forming the amphiphilic product (fig. 7.1) [81].

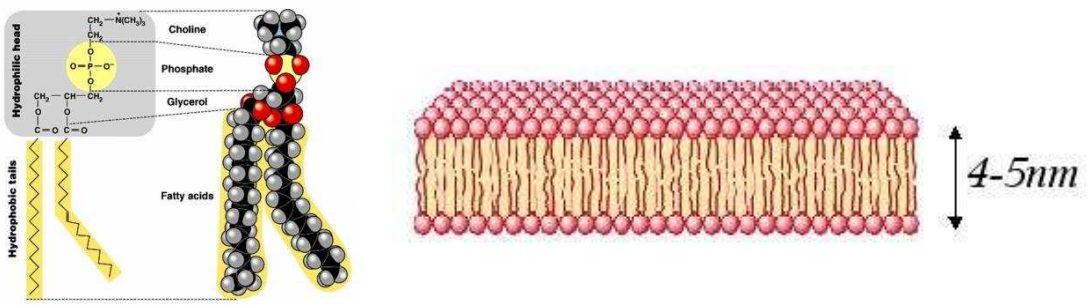

Figure 7.1: Left: POPC (palmitoyl-oleoyl phosphatidylcholine) molecule made of a polar choline head, a phosphate, one saturated C16 and one C18:1 unsaturated hydrophobic tail. Right: self-assembly of phospholipid molecules in a planar bilayer.

A given phospholipid is characterized by its gel-liquid main transition temperature T_m, separating a fluid, disordered region on the one hand, from a viscous and better ordered region on the other hand. The transition is accompanied by a clear calorimetric signal (peak of specific heat observed in differential scanning calorimetry experiments) [82]. Transition temperatures T_m spread over a wide range of values, and are determined to a large extent by the length of the hydrocarbonated tails and the presence of insaturations (double *cis* C=C bonds) along the chains. Equimolar mixtures of phospholipids comprising one component forming a pure liquid phase, and one component forming a pure gel phase do not mix homogeneously [82].

Ternary cholesterol-phospholipid mixtures have been studied in great detail, as they are considered as model systems regarding lateral lipid segregation phenomena. Fluorescence microscopy observations

reveals the existence of large domains with distinct composition. Such lateral segregations could be related with the nanometric sized heterogeneities (rafts) that presumably exists in biological membranes, while presenting noticeable differences, especially regarding their size.

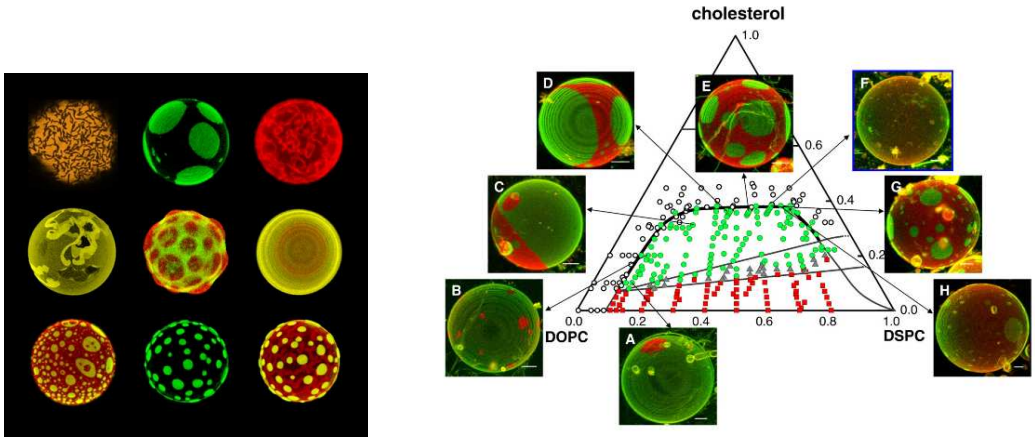

Figure 7.2: Left: selection of beautiful confocal fluorescence microscopy images representing domains in giant vesicles, from Luis Bagatolli web site, see *e.g.* [83]. Right: experimental ternary phase diagram DPPC/DOPC/Chol. obtained by Zhao *et al.* [84].

With Jean Wolff, postgraduate student, we started to investigate the nature of phase equilibria in binary and ternary phospholipid mixtures, with the aim of proposing a robust and predictive model for establishing thermodynamic phase diagrams. Our approach combines ideas from statistical physics (discrete spin models) and thermodynamics (regular solution approach, thermodynamic potentials) similar in spirit to a model introduced by Komura et al. [85]. Our results are very encouraging, with a fast and efficient numerical method for finding ternary phase coexistence domains (figs. 7.2 and 7.3) [86]. I outline below a few possible future directions in line with this topic.

Predicting phase equilibria

One of our goals is to develop a tool for predicting the phase coexistence (Gibbs diagram) of a mixture of arbitrary composition comprising phospholipids and cholesterol. There are two possible approaches.

- In the geometrical approach, each molecule is described by its geometrical attributes: volume or molecular mass of the polar head groups, length of the acyl chains, number of insaturations, charges and electric dipoles. . . .
- In the thermodynamic approach, one builds a model based on the properties of pure lipid phases: melting temperature T_m, enthalpy change at the transition ΔH. . .

Our current approach combines thermodynamic features of phospholipids, with geometrical aspects such as the excluded volume attributed to cholesterol molecules. We plan to check the robustness and predictive power of our model on the various known systems. Our model will hopefully be regarded as helpful for guiding experimentalists towards creating mixtures with optimal composition.

Accounting for correlations

Our current description of the lipid mixing properties is a mean-field one. The phospholipid mixtures of interest, however, display regions with critical fluctuations of composition, including one or two critical points (fig. 7.2). The existence of critical regions, and their possible biological implications is a challenging perspective [87]. Do the critical regions help biological membranes with changing and adapting their compositions in response to external factors ? Do they change the solubility of nanoobjects or macromolecules in the membrane ? Critical fluids are usually considered as excellent solvents.

It would be interesting to extend liquid state concepts, for instance integral equations [88, 89], or lattice fluid approaches, such as the SCOZA [90] to the above mentioned geometrical and thermodynamic models. Accounting for spatial correlations of lipids will modify the coexistence lines in the associated

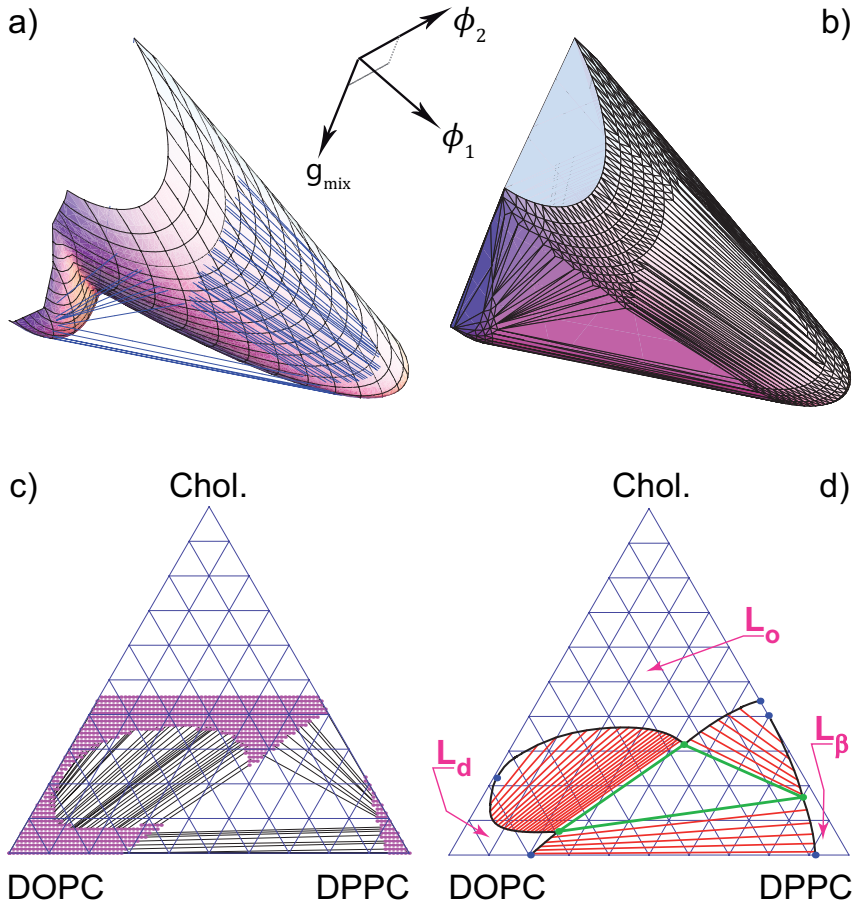

Figure 7.3: A combination of numerical and analytical calculations lead us to a well-defined and convincing ternary phase diagram [86].

Gibbs diagrams. Alternatively, one may consider sampling the configuration space of these lattice models with suitable Monte-Carlo approaches [82, 91].

Dynamical and thermodynamic role of polydispersity

Owing to the Gibbs phase rule, increasing the number of chemical species increases the number of possible coexisting phases and the complexity of the resulting phase diagram, the determination of which becoming a formidable task [92].

Biological membranes contain hundreds of different molecules, with uneven proportions. We can formulate various explanations regarding this huge chemical diversity:

- The large number of observed lipid molecules is just a by-product of the random activity of enzymes involved in the metabolism and the regulation of lipid species, with no defined purpose.
- The large number of lipid molecules does not originate from thermodynamics or phase equilibria considerations, but from chemical considerations (say *e.g.* complex signaling cascades and metabolic pathways...).
- The large number of lipid molecules reflects a physical requirement related to thermodynamics in a way that must be understood: criticality, fluctuations of composition, microphase separation...

Our statistical approach can be used to scrutinize the third hypothesis, showing how changing the number of participating chemical species changes the thermodynamic properties of the mixtures. Dynamical properties (*e.g.* spinodal decomposition [93]) in the presence of a large number of components might teach us something regarding the size of the resulting domains and rafts.

To end up, it will be interesting to consider systems of variable composition, such as membranes containing photoactivable molecules able to oxidize the unsaturated lipid species, therefore changing their physical properties during the course of the experiment [94, 95].

7.2 Diffusion dominated dynamics

Bridging dynamics and adhesion

Soft matter physics offers numerous examples of situations involving exploratory random dynamics coupled to reaction or capture phenomena (see Section 4.1, page 23). Members of our group worked on the bridging kinetics of tethered ligands attached to the end of a polymer chain [96, 97]. With W.G. Dantas, postdoctoral fellow, we started to study the distribution of first contact times between a sticking membrane and a flat rigid surface (fig. 7.4(c)), a subtle problem given the importance of the hydrodynamic effects and the bidimensional elastic character of the object. This problem is linked with adhesion experiments performed in our group, as well as with other published experimental results [98] or theoretical models [99, 100].

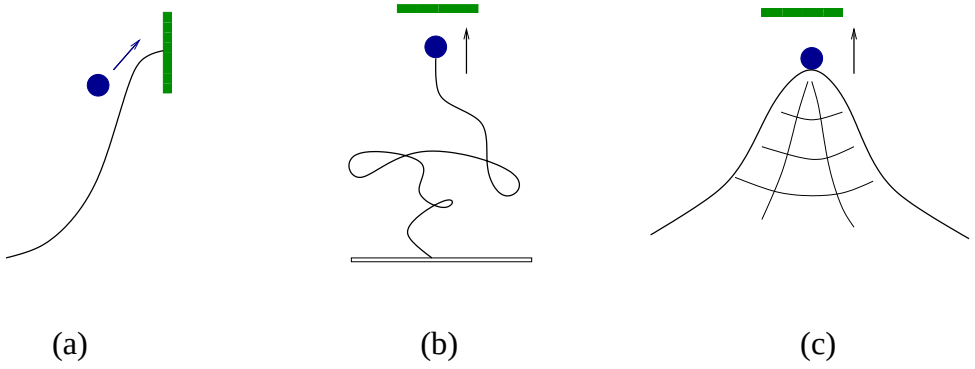

Figure 7.4: (a) Capture of a Brownian diffusive particle subject to a repulsive barrier. (b) Bridging of a ligand grafted at the end of a polymer chain. (c) Bridging of a ligand grafted on an elastic or smectic surface.

Theory and simulation

The problem mentioned in fig. 7.4(c) is far from having received a satisfactory answer, whether one considers it from an analytical or from a numerical point of view. We are interested in systems (tethered ligand bridging, nucleation and propagation of membrane adhesion) differing from the standard barrier crossing situation (*e.g.* the Kramers escape problem), due to the somewhat non standard diffusion regime (compact subdiffusive Brownian exploration according to de Gennes [41]) and to the role of hydrodynamics (bridging of tethered ligands under shear conditions, lubrication flows near unpenetrable walls [101]).

We might consider trying on these problems some recently proposed innovative methods for computing reaction rates [8] and compare the resulting simulations results with various analytical approaches (ongoing collaboration with A. Johner, C. Marques, W.G. Dantas).

Correlation and fluorescence transfer

Correlation fluorescence spectroscopy (FCS) is a technique consisting in tracking the fluorescence intensity fluctuations coming from a small illuminated volume. The number of fluorophores located at the vicinity of the focal point of the illuminating beam fluctuates randomly, in a way that informs us on the diffusion dynamics of these fluorescent probes [102, 103, 104]. On the other hand, resonance energy transfer (RET) between pairs of fluorescent molecules is a powerful tool for probing the spatial colocalization between acceptor and donor molecules, with a precision of a few nanometers (Förster radius) [103, 104].

I propose to investigate the statistical properties of the fluorescence emission signal resulting from the random motion of donor and acceptor molecules diffusing freely at the surface of a liposome or a vesicle. It would be interesting to know, as it is the case with FCS, if one can determine in this way the diffusion

properties of the fluorescent tracers, and perhaps reveal the presence of dynamical heterogeneities in the membranes [105].

The algorithm presented in Section 3.2 is suitable for the simulating transient fluorescence transfer phenomena, the Förster radius being substituted for the capture radius. Photobleaching degradation of fluorophores may also be easily accounted for within this framework. It will there be stimulating to imagine new experimental schemes with the aim of probing the short time scales diffusing dynamics of the phospholipid constituents.

Chapitre 8

Physique statistique de mélanges phospholipides et dynamique de membrane

Le projet de recherche comporte deux volets. Le premier concerne les équilibres de phase dans les mélanges de phospholipides. Le second se situe dans la continuité de nos approches de réaction-diffusion pour la cinétique d'association de molécules complémentaires, le mécanisme d'adhésion des membranes et la dynamique des phénomènes de fluorescence.

8.1 Séparation de phases dans les bicouches de phospholipides

Les phospholipides comptent parmi les constituants majeurs des membranes biologiques. Ces molécules tensioactives s'assemblent spontanément en milieu aqueux sous forme de phases uni ou multilamellaires, dont on peut relativement bien contrôler la morphologie en laboratoire. Les vésicules géantes unilamellaires se prêtent bien par exemple à l'étude des propriétés mécaniques et d'adhésion des membranes.

Il existe dans le vivant une grande variété de phospholipides aux propriétés physico-chimiques très diverses. Cette diversité provient de leur structure chimique "modulaire", autorisant une vaste combinatoire des composants hydrophiles et hydrophobes de ces molécules (Figure 8.1) [81].

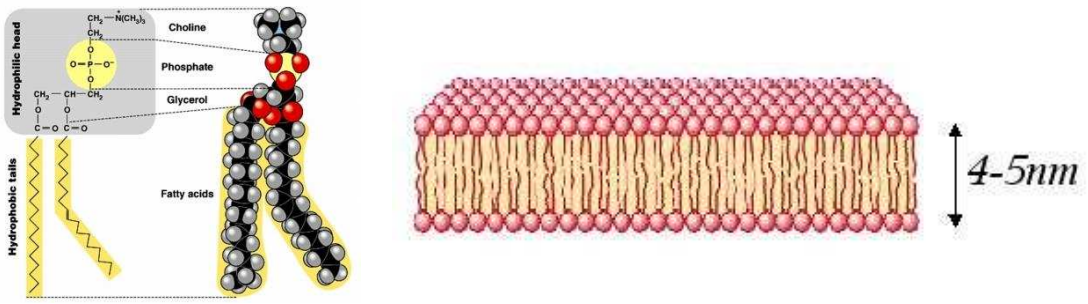

FIG. 8.1 – A gauche : molécule de POPC (palmitoyl-oleoyl phosphatidylcholine) constituée d'une tête polaire choline, d'un phosphate, d'une queue hydrophobe saturée C16 et d'une queue insaturée C18 :1. A droite : autoassemblage de phospholipides en une bicouche plane.

Une molécule phospholipide donnée est caractérisée par l'existence d'une température de transition liquide-gel T_m, séparant d'une part un domaine fluide et désordonné et de l'autre un domaine visqueux et mieux ordonné, et qui se caractérise par l'existence d'un signal calorimétrique marqué (pic de chaleur spécifique). Les températures T_m varient sur une gamme étendue et sont pour une large part déterminées par la longueur des chaînes hydrocarbonées, ainsi que par la présence d'insaturations (doubles liaisons *cis* C=C) le long de ces chaînes. Il n'est pas possible d'obtenir de phase homogène à partir d'un mélange équimolaire de phospholipides dont l'un serait dans sa phase liquide et l'autre dans sa phase gel [82].

Les mélanges ternaires phospholipides-cholestérol font l'objet d'études approfondies du fait de leur rôle de membranes artificielles modèle, c'est-à-dire de membranes de composition connue et proches de certaines membranes biologiques. L'observation par microscopie de fluorescence sur des vésicules géantes permet de mettre en évidence l'existence de large domaines de composition distincte. Ces ségrégations latérales semblent avoir un lien avec les hétérogénéités nanométriques (rafts) observées dans les membranes biologiques, tout en présentant des différences notables, en particulier de taille, avec celles-ci.

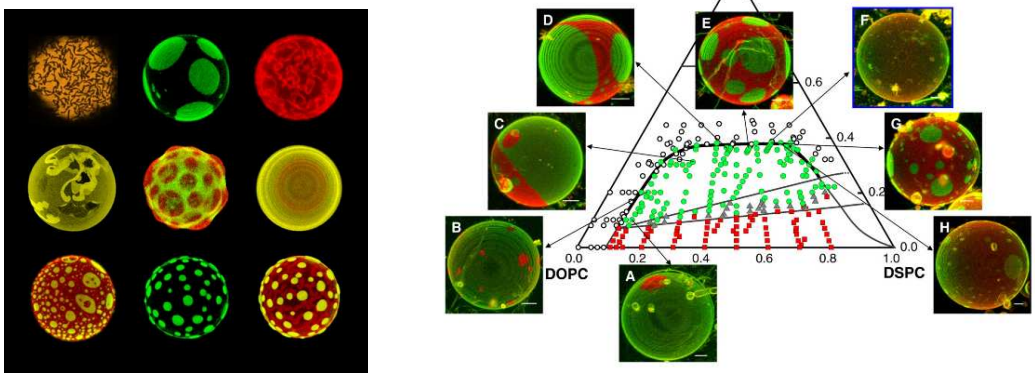

FIG. 8.2 – A gauche : sélection de belles images de microscopie confocale de fluorescence montrant des domaines dans des vésicules géantes, vue sur le site internet de Luis Bagatolli, voir *e.g.* [83]. A droite : diagramme de phase ternaire expérimental DPPC/DOPC/Chol obtenu par Zhao *et al.* [84].

Nous avons entrepris avec Jean Wolff, doctorant, de comprendre la nature des équilibres de phase de mélanges binaires et ternaires de phospholipides, et de proposer des modèles robustes et prédictifs pour ces équilibres. Notre approche combine des concepts de physique statistique (modèle d'Ising et ses généralisations), de thermodynamique (théorie des solutions régulières, potentiels thermodynamiques) et de physique des liquides (interaction de volume exclu, de Van der Waals), similaire dans l'esprit à l'approche de Komura et al. [85]. Nos résultats sont très encourageants, avec une méthode rapide et efficace pour trouver les domaines de coexistence des mélanges ternaires (fig. 8.2 et 8.3) [86]. Je détaille ci-dessous les principales pistes à explorer dans la continuité de cette thématique.

Prédiction des équilibres de phases

Notre but est de développer un outil permettant de prédire l'allure du diagramme de coexistence (diagramme de Gibbs) d'un mélange arbitraire de phospholipides (et éventuellement cholestérol). Pour cela il y a deux approches.

- Dans l'approche géométrique, chaque molécule est décrite par des attributs de nature géométrique : volume ou masse molaire des têtes polaires, longueur des chaînes hydrocarbonées, nombre d'insaturations, volume des molécules, charges et dipôles électriques...
- Dans l'approche thermodynamique, on se base sur les propriétés thermodynamiques des lipides purs : température de changement d'état T_m, chaleurs latentes à la transition ΔH...

Notre approche actuelle combine l'aspect thermodynamique pour les phospholipides et un concept original de volume exclu pour le cholestérol. Nous comptons tester la robustesse et la capacité prédictive de cette approche sur l'ensemble des mélanges thermodynamiques déjà connus. Notre modèle sera, nous l'espérons, considéré comme utile par les expérimentateurs pour définir des mélanges de lipides aux propriétés optimales.

Prise en compte des corrélations

Notre description des propriétés de mélanges de lipides est une approche de champ moyen. Les mélanges phsopholipides les plus intéressants présentent des fluctuations critiques de composition avec un ou deux points critiques (fig. 8.2). L'existence de ces régions critiques, et leur éventuelle pertinence biologique est une perspective très interessante [87]. Ces régions critiques sont-elles là pour aider les membranes biologiques à adapter leur composition en fonction de facteurs extérieurs ? Les fluides critiques

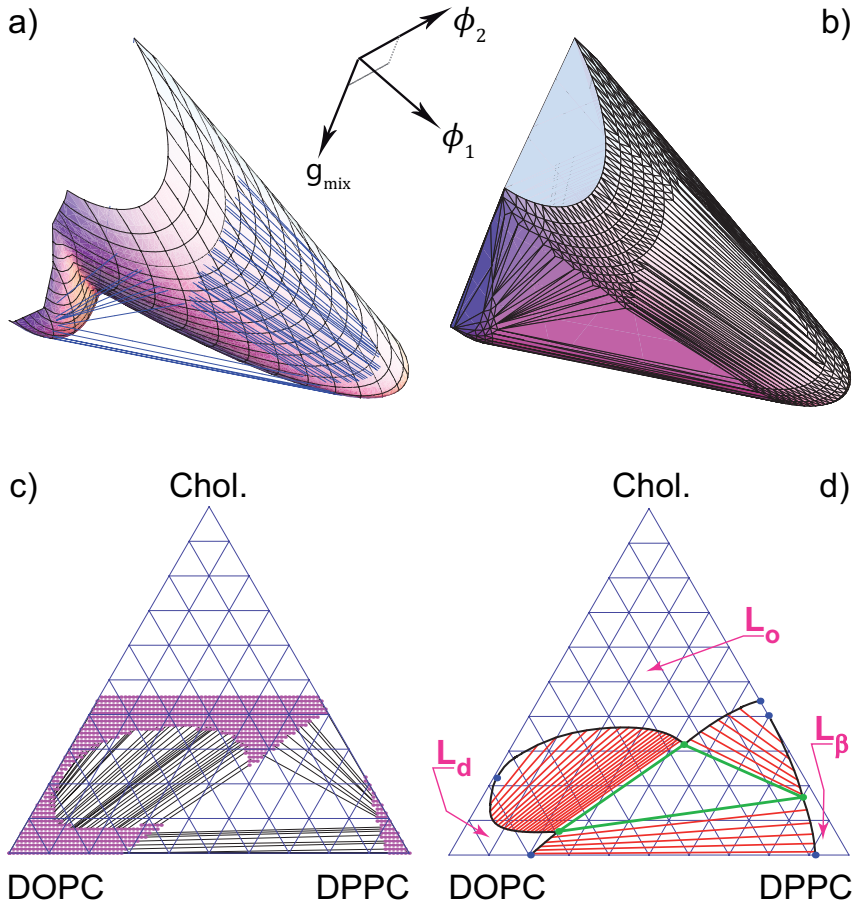

FIG. 8.3 – Une combinaison de calculs numérique et analytiques nous a mené à des diagrammes de phase ternaires bien définis et convaincants [86].

sont connus pour être de remarquables solvants, et la capacité d'une membrane lipidique à adsorber des nanoobjets ou macromolécules étrangères est susceptible de s'en trouver accrue.

Je souhaiterais étendre les approches de théorie de liquides, comme les équations intégrales [88, 89] ou de fluides sur réseau, comme la SCOZA (Self-Consistent Ornstein-Zernike Approximation) [90] aux modèles géométriques et thermodynamiques de lipides décrits dans la partie précédente. La prise en compte des corrélations de position entre lipides aura pour conséquence de modifier le tracé des lignes de coexistence dans les diagrammes. D'autre part nous pourrons échantilloner ces modèles sur réseau avec l'aide de méthodes de Monte-Carlo appropriées [82, 91].

Influence dynamique et thermodynamique de la polydispersité

En vertu de la règle des phases de Gibbs, augmenter le nombre d'espèces chimiques augmente le degré de coexistence possible et la complexité des diagrammes de phase, dont la détermination devient rapidement délicate [92]. Les membranes biologiques naturelles contiennent des dizaines de molécules, mais en proportions inégales. Nous pouvons formuler plusieurs hypothèses quant à la raison d'une telle diversité chimique :

- La variété de molécules observées n'est que l'incidence de l'activité aléatoire d'enzymes chargés de la synthèse des phospholipides, mais ne répond pas à une finalité particulière.
- La variété de molécules observées répond à une nécessité qui ne relève ni de la thermodynamique, ni d'un quelconque équilibre de phases, mais plutôt des propriétés chimiques de ces molécules.
- La variété de molécules observées répond à un impératif d'ordre thermodynamique qu'il importe de comprendre : criticalité, fluctuations de composition, microséparation de phase...

L'approche statistique que nous proposons devrait permettre d'examiner la troisième hypothèse, en montrant comment l'augmentation du nombre d'espèces chimiques modifie les propriétés de coexistence

du mélange. Les propriétés dynamique (décomposition spinodale [93]) en présence d'un grand nombre de composants pourraient s'avérer instructives vis-à-vis de la taille des domaines, ou rafts, obtenus.

Pour finir, il sera intéressant de discuter la situation de mélanges dont la composition évolue au cours du temps, comme par exemple, lors de l'utilisation de molécules photoactivables qui dégradent les phospholipides sous irradiation [94, 95].

8.2 Dynamique dominée par la diffusion

Dynamique de pontage et adhésion

La physique de la matière molle abonde de situations mettant en jeu une dynamique exploratoire diffusive couplée à des mécanismes de réaction ou de capture (voir section 4.1, page 23).

Des membres de notre groupe ont étudié la cinétique de pontage d'un ligand situé en bout de chaîne polymère [96, 97]. Nous avons entrepris avec W.G. Dantas (post-doctorant) d'étudier la distribution des temps de premier contact entre une membrane adhésive et un substrat rigide plan (Figure 7.4(c)), problème délicat compte-tenu de l'importance des effets hydrodynamiques et de la dynamique de l'objet élastique bidimensionnel. Ce problème est lié aux expériences d'adhésion menées dans notre groupe, ainsi qu'à divers autres résultats théoriques [99, 100] et expérimentaux [98] publiés.

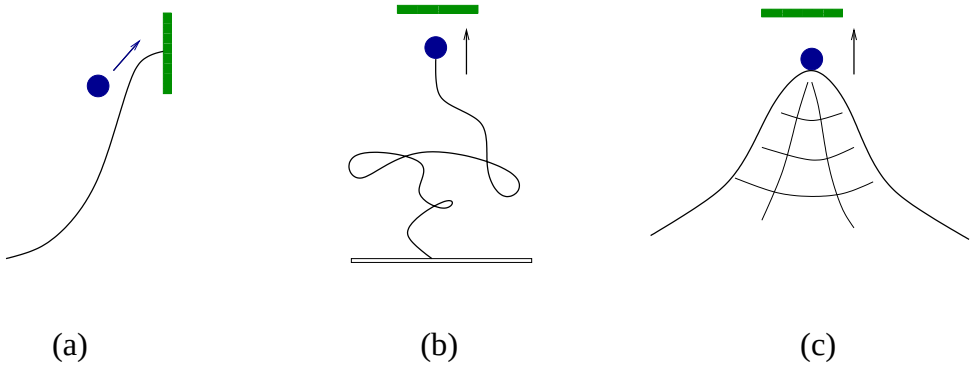

FIG. 8.4 – (a) Capture d'une particule diffusive Brownienne soumise à une barrière de potentiel. (b) Pontage d'un ligand en bout de chaîne polymère. (c) Pontage d'un ligand greffé sur une surface élastique ou smectique.

Théorie et simulation

Le problème représenté sur la figure 7.4(c) est loin d'avoir reçu une réponse satisfaisante, que ce soit d'un point de vue analytique ou numérique. Nous nous intéressons à des systèmes (pontage de ligand en bout de chaîne, nucléation et propagation de l'adhésion d'une membrane) qui diffèrent de la situation habituelle de franchissement de barrière réactionnelle (problème de Kramers) à cause du caractère inhabituel du régime diffusif (exploration Brownienne compacte sous diffusive selon de Gennes [41]) et du rôle particulier de l'hydrodynamique (pontage de ligands sous cisaillement, écoulement de lubrification près des parois [101]).

Il devrait être possible d'adapter des méthodes de simulation innovantes pour calculer ces taux de réaction [8] et comparer le résultats des simulations aux diverses approaches analytiques (travail en cours avec A. Johner, C. Marques, W.G. Dantas).

Corrélation et transfert de fluorescence

La spectroscopie de corrélation de fluorescence (FCS) consiste à étudier les fluctuations d'intensité de fluorescence au foyer d'un faisceau lumineux excitateur. Le nombre de fluorophores contenus à chaque instant au foyer du faisceau fluctue fortement en raison de la mobilité des fluorophores. Cela permet de mesurer la constante de diffusion de ces fluorophores, agissant comme sonde locale [102, 103, 104]. D'autre part, le transfert résonant d'énergie (FRET) entre paires de fluorophores, est un outil remarquable

permettant de colocaliser les fluorophores donneur et accepteur avec une précision de l'ordre de quelques nanomètres (rayon de Förster) [103, 104].

Je propose d'explorer les propriétés statistiques du signal de fluorescence émis au cours du mouvement d'exploration aléatoire de molécules donneuses et accepteuses diffusant librement à la surface d'une vésicule ou d'un liposome. Il serait intéressant de savoir si l'on peut ainsi remonter aux propriétés de diffusion des marqueurs fluorescents, et peut-être de révéler ainsi la présence d'hétérogénéités dynamiques dans les membranes [105]. Les algorithmes présentés en section 3.2 se prêtent bien à la simulation de phénomènes de transfert de fluorescence transitoires, le rayon de Förster se substituant au rayon de capture. La dégradation par photoblanchiment des fluorophores peut également être prise en compte. Il sera stimulant d'imaginer de nouveaux protocoles expérimentaux ayant pour but d'observer les phénomènes de diffusion aux petites échelles des composés phospholipides.

Part III

Personal data

Chapter 9

Curriculum Vitæ, publications

9.1 Curriculum Vitæ

Research experience

- Assistant professor at the University of Strasbourg, member of the Institut Charles Sadron, *since Nov. 2005*
  Theory of Soft Condensed Matter Systems

- Assistant professor at the University of Strasbourg (formerly Université Louis Pasteur), member of the LDFC (Laboratory of Complex Fluid Dynamics), in the team of Dr H. Isambert, *Sept. 2001-Nov. 2005.*
  Statistical study and prediction of RNA secondary structures

- Research Assistant at the Department of Physics and Astronomy, University of Manchester, UK, working with Prof. M.A. Moore, *Sept. 1999- Aug. 2001*
  Thermodynamics of the structural glass transition

- Visiting fellow at the Physics Department, Indian Institute of Science, Bangalore, India, working with Prof. Chandan Dasgupta. *Dec. 1998-June. 1999*
  Phase behaviors of fluids with quenched disorder

Education

- Doctorate in Physics, Université J. Fourier, Grenoble, France, under the supervision of D. Feinberg.
  Theme: Phenomenology of high-Tc superconductors and glassy dynamics, Sept. 1998, awarded with honors

- Graduation from ENS Lyon *1991-1994*: DEA (M.Sc) in theoretical physics *1994*, Licence (B.Sc) in physics *1992*, Licence (B.Sc) in mathematics *1993*.

9.2 Publications and Communications

Publications in international journals with peer review

A1 **F. Thalmann**.
Activated drift motion of a classical particle with a dynamical pinning effect.
European Physical Journal B, 3:497, 1998.

A2 **F. Thalmann**, C. Dasgupta, and D. Feinberg.
Phase diagram of a classical fluid in a quenched random potential.
EuroPhysics Letters, 50(1):54–60, 2000.

A3 **F. Thalmann**.
Geometrical approach for the mean-field dynamics of a particle in a short-range correlated random potential.
European Physical Journal B, 19:49–63, 2001.

A4 **F. Thalmann**.
Aging and non-linear glassy dynamics in a mean field model.
European Physical Journal B, 19:65–73, 2001.

A5 **F. Thalmann**.
Note on the role of dimensionality in the structural glass transition.
Journal of Chemical Physics, 116(8):3378, 2002.

A6 A. Xayaphoummine, T. Bucher, **F. Thalmann**, and H. Isambert.
Prediction and statistics of pseudoknots in RNA structures using exactly clustered stochastic simulations.
PNAS, 100(26):15310–15315, december 2003.

A7 D.J. Durian, H. Bideaud, P. Duringer, A. Schröder, **F. Thalmann**, and C.M. Marques.
What is a pebble shape ?
Physical Review Letters, 97:028001, 2006.

A8 V.A. Baulin, C.M. Marques, and **F. Thalmann**.
Collision induced spatial organization of microtubules.
Biophysical Chemistry, 128:231–244, 2007.

A9 **F. Thalmann** and J. Farago.
Trotter derivation of algorithms for Brownian and dissipative particle dynamics.
Journal of Chemical Physics, 127:124109, 2007.

A10 N.-K. Lee, A. Johner, **F. Thalmann**, L. Cohen-Tannoudji, E. Bertrand, J. Baudry, J.Bibette, and C.M. Marques
Ligand receptors interactions in chains of colloids: When reaction are limited by rotational diffusion.
Langmuir, 24(4):1296, 2008.

A11 L. Cohen-Tannoudji, E. Bertrand, J. Baudry, C. Robic, M. Pellissier, A. Johner, **F. Thalmann**, N.-K. Lee, C.M. Marques, J. Bibette
Measuring the kinetics of biomolecular recognition with magnetic colloids.
Physical Review Letters, 100(10):108301, 2008.

A12 **F. Thalmann** and N.-K. Lee
Fast algorithms for $X \to 0$ reaction-diffusion algorithms
Journal of Chemical Physics, 130(7):074102 (2009).

A13 C. Arnold, **F. Thalmann**, C.M. Marques, P. Marie and Y. Holl
Surfactant Distribution in Waterborne Acrylic Films I. Bulk Investigation *Journal of Physical Chemistry B*, 114(28):9135-9147 (2010).

A14 **F. Thalmann**.
A schematic model for molecular affinity and binding with Ising variables.
European Physical Journal E, 31:441-454 (2010).

A15 G. Nam, M.-L. Hisette, Y. Sun, T. Gisler, A. Johner, **F. Thalmann**, A.P. Schröder, C.M. Marques and N.-K. Lee.
Scraping and stapling of end-grafted DNA chains by a bio-adhesive spreading vesicle reveal chain internal friction and topological complexity.
Physical Review Letters, 105(8):088101 (2010)

Submitted papers

S16 Carlos Mendoza, Carlos M. Marques and **F. Thalmann**.
Enhanced shear separation for chiral magnetic colloidal aggregates.
submitted to *Physical Review Letters*.

S17 **F. Thalmann**, V. Billot and C.M. Marques.
Lipid bilayer adhesion on sparse DNA carpets: theoretical analysis of membrane deformations induced by single end-grafted polymers.
submitted to *Physical Review E.*.

S18 J. Wolff, C.M. Marques and **F. Thalmann**.
A thermodynamic approach to phase coexistence in ternary Cholesterol-phospholipid mixtures.
submitted to *Physical Review Letters*.

Publications in national journal with peer review

B1 **F. Thalmann**.
Électrostatique et probabilités.
Bulletin de l'Union des Professeurs de Physique et Chimie (UdPPC) 103:91, November 2009.

Oral presentations, 2006-2010

O1 Jourées de la matière condensée, Société Française de Physique - JMC 11, 25-29 Aug. 2008

O2 APS March Meeting, Pittsburgh, USA, March 2009

O3 44^{th} Meeting of the German Colloid Society, Hamburg, Germany, 28-30 Sept. 2009

O4 Jourées plénière GDR CellTiss, Dourdan, France, 26-28 Oct. 2009

O5 Jourées de Physique Statistique, Paris, France, 28-29 Jan. 2010

O6 467th Wilhelm and Else Heraeus Seminar, Biophysics of membrane transformations, 26-30 Oct. 2010 (*planned*)

9.3 Main collaborations in the past 4 years

⋆ **J. Farago**.
ICS, CNRS, Université de Strasbourg, Strasbourg, France

⋆ **A. Johner**.
ICS, CNRS, Université de Strasbourg, Strasbourg, France

⋆ **C. Marques**.
ICS, CNRS, Université de Strasbourg, Strasbourg, France

⋆ **N.-K. Lee**.
Sejong University, Seoul, South-Korea

⋆ **V. Baulin**.
Universitat Rovira et Virgili, Tarragona, Spain

⋆ **C. Mendoza**.
Dep. Materiales, UNaM, Mexico DF, Mexico

9.4 Teaching and Responsabilities

Bachelor of Science (*Licence*) and *Masters* were introduced in Strasbourg in 2005, replacing the older *DEUG, Licence, Maîtrise* curriculum. **Université Louis Pasteur** has become **Université de Strasbourg** since January 2009. I am attached to the physics department, currently referred as the **UFR de Sciences Physiques et Ingéniérie**.

Undergraduate

- Tutorials in Quantum Mechanics ("TD Maîtrise" - 4^{th} year)
- Tutorials in Statistical Physics ("TD Maîtrise" - 4^{th} year)
- Tutorial in Introductory Physics (1^{st} year)
- Tutorial in Thermodynamics (2^{nd} year)

Postgraduate

- Course on Hydrodynamics of Complex Fluids and Brownian Processes (with C.M. Marques, *Master of Condensed Matter and Nanophysics*)
- Training courses for the French national *Agregation de Science Physiques, Option Physique* competitive examination, preparation of the written exam.
- Introduction to statistical physics, *Master of Material Sciences*.

Responsabilities

- Elected member of the UFR Council since 2003.

9.5 Student supervision

Ph.D student

1. Jean WOLFF (joint supervision with Carlos Marques, HDR)
   Phase separation in self-assembled bilayers since Sept. 2009.

Master students

1. Axel GROMER, DEA de Matière Condensée et Nanophysique, Strasbourg:
   Hydrodynamic interactions in colloids: translation/rotation coupling,2004
2. Jean WOLFF Master Physique M2, parcours Physique de la Matière Condensée:
   Phase separation in giant phospholipid vesicles, 2009

Undergraduate students

1. Patrick SOMMERS, Maîtrise de Mathématiques Appliquées:
   Numerical simulation of pebble wearing, 2003
2. Faïçal SAIQ, Maîtrise de Physique (with Michel Rausch de Traubenberg)
   Representations and products of representation of $SU(2)$ *with Schwinger bosons*,2005
3. Lucie MULLER Licence MPC (Maths-Physique-Chimie) L3:
   Fluorescence transfer and quenching in phospholipid membranes, 2010

Bibliography

[1] Maddalena Venturoli, Maria Maddalena Sperotto, Marieke Kranenburg, and Berend Smit. Mesoscopic models of biological membranes. *Physics Reports*, 437:1–54, 2006.

[2] Sandra V. Bennun, Matthew I. Hoopes, Chenyue Xing, and Roland Faller. Coarse-grained modeling of lipids. *Chemistry and Physics of Lipids*, 159(2):59 – 66, 2009.

[3] Ira R. Cooke, Kurt Kremer, and Markus Deserno. Tunable generic model for fluid bilayer membranes. *Phys. Rev. E*, 72(1):011506, Jul 2005.

[4] Roland Faller and Siewert-Jan Marrink. Simulation of domain formation in dlpc−dspc mixed bilayers. *Langmuir*, 20(18):7686–7693, 2004.

[5] Olaf Lenz and Friederike Schmid. Structure of symmetric and asymmetric "ripple" phases in lipid bilayers. *Phys. Rev. Lett.*, 98(5):058104, Jan 2007.

[6] P.J. Hoogerbrugge and J.M.V.A. Koelman. Simulating microscopic hydrodynamic phenomena with dissipative particle dynamics. *EuroPhysics Letters*, 19:155, 1992.

[7] Pep Espanol. Hydrodynamics from dissipative particle dynamics. *Physical Review E*, 52(2):1734, 1995.

[8] Daan Frenkel and Berend Smit. *Understanding Molecular Simulations: From Algorithms to Applications*. Academic Press, 2002.

[9] Song-Ho Chong, Martin Aichele, Hendrik Meyer, Matthias Fuchs, and Jörg Baschnagel. Structural and conformational dynamics of supercooled polymer melts: Insights from first-principles theory and simulations. *Phys. Rev. E*, 76(5):051806, Nov 2007.

[10] Pep Espanol and Patrick Warren. Statistical mechanics of dissipative particle dynamics. *Europhysics Letters*, 30:191, 1995.

[11] J. Bonet Avalos and A. D. Mackie. Dynamic and transport properties of dissipative particle dynamics with energy conservation. *Journal of Chemical Physics*, 111(11):5267, 1999.

[12] D.L. Ermak and H. Buckholz. Numerical integration of the langevin equation: Monte-carlo simulation. *Journal of Computational Physics*, 35:169–182, 1980.

[13] Axel Brunger, Charles L. Brooks, and Martin Karplus. Stochastic boundary conditions for molecular dynamics simulations of st2 water. *Chemical Physics Letters*, 105(5), 1984.

[14] Andrea Ricci and Giovanni Ciccoti. Algorithms for brownian dynamics. *Molecular Physics*, 101(12):1927–1931, June 2003.

[15] P Allen and P Tildesley. *Numerical simulation*. Oxford, 1986.

[16] I. Pagonabarraga, M.H.J. Hagen, and D. Frenkel. Self-consistent dissipative particle dynamics algorithm. *Europhysics Letters*, 42:377, 1998.

[17] Tony Shardlow. Splitting for dissipative particle dynamics. *SIAM Journal of Scientific Computing*, 24:1267–1282, 2003.

[18] P. Nikunen, M. Karttunen, and I. Vattulainen. How would you integrate the equations of motion in dissipative particle dynamics simulations ? *Computer Physics Communication*, 153:407–423,, 2003.

[19] M. Serrano, G. De Fabritiis, P. Español, and P.V. Coveney. A stochastic trotter integration scheme for dissipative particle dynamics. *Mathematics and Computers in Simulation*, 72:190, 2006.

[20] G. De Fabritiis, M. Serrano, P Espanol, and P.V. Coveney. Efficient numerical integrators for stochastic models. *Physica A*, 361, 2006.

[21] J Stoer and R Bulirsch. *Introduction to Numerical Analysis*. Text in applied mathematics 12. Springer, 2nd edition edition, 1991.

[22] Fabrice Thalmann and Jean Farago. Trotter derivation of algorithms for brownian and dissipative particle dynamics. *Journal of Chemical Physics*, 127:124109, 2007.

[23] P.E. Kloeden and E. Platen. *The Numerical Solution of Stochastic Differential Equations*. Springer-Verlag, 1999.

[24] Etienne Forest and Ronald D. Ruth. Fourth-order symplectic integration. *Physica D*, 43:105–117, 1990.

[25] Masuo Susuki. Nonsymmetric higher-order decomposition of exponential operators and symplectic integrators. *Journal of the Physical Society of Japan*, 61(9):3015–3019, 1992.

[26] Masuo Suzuki. General theory of higher-order decomposition of exponential operators and symplectic operators. *Physics Letters A*, 165:387–395, 1992.

[27] Hasuo Yoshida. Construction of higher order symplectic operators. *Physics Letters A*, 150:262, 1990.

[28] Jacques Laskar and Philippe Robutel. High order symplectic integrators for perturbed hamiltonian systems. *Celestial Mechanics nad Dynamical Astronomy*, 80(1):39–62, 2001.

[29] K. Burrage and P.M. Burrage. High strong order methods for non-commutative stochastic ordinary differential equation systems and the Magnus formula. *Physica D*, 133:34, 1999.

[30] Eric Vanden-Eijnden and Giovanni Ciccotti. Second-order integrators for langevin equations with holonomic constraints. *Chemical Physics Letters*, 429:310–316, 2006.

[31] Masao Doi. Second quantization representation for classical many-particle system. *Journal of Physics A*, 9(9):1465, 1976.

[32] Masao Doi. Stochastic theory of diffusion-controlled reaction. *Journal of Physics A*, 9(9):1479, 1976.

[33] Daniel C. Mattis and M. Lawrence Glasser. The uses of quantum field theory in diffusion-limited reactions. *Rev. Mod. Phys.*, 70(3):979, Jul 1998.

[34] Luca Peliti. Path integral approach to birth-death process on a lattice. *Journal de Physique*, 46:1469–1483, 1985.

[35] Robert A. Alberty and Gordon G. Hammes. Application of the theory of diffusion-controlled reactions to enzyme kinetics. *Journal of Physical Chemistry*, 62:154, 1958.

[36] Pierre Bongrand. Ligand-receptor interactions. *Report on Progress in Physics*, 62:921–968, 1999.

[37] A. Koenig, P. Hébraud, C. Gosse, R. Dreyfus, J. Baudry, E. Bertrand, and J. Bibette. Magnetic force probe for nanoscale biomolecules. *Phys. Rev. Lett.*, 95(12):128301, Sep 2005.

[38] L. Cohen-Tannoudji, E. Bertrand, J. Baudry, C. Robic, C. Goubault, M. Pellissier, A Johner, F Thalmann, N.-K Lee, C.M. Marques, and J. Bibette. Measuring the kinetics of biomolecular recognition with magnetic colloids. *Physical Review Letters*, 100, 2008.

[39] Gerald Wilemski and Marshall Fixman. General theory of diffusion-controlled reactions. *Journal of Chemical Physics*, 58(9):4009, 1973.

[40] Gerald Wilemski and Marshall Fixman. Diffusion-controlled intrachain reactions of polymers: I theory. *Journal of Chemical Physics*, 60(3):866, 1974.

[41] P. G. de Gennes. Kinetics of diffusion-controlled processes in dense polymer systems. i. nonentangled regimes. *The Journal of Chemical Physics*, 76(6):3316–3321, 1982.

[42] Marcos, Henry C. Fu, Thomas R. Powers, and Roman Stocker. Separation of microscale chiral objects by shear flow. *Physical Review Letters*, 102(15):158103, 2009.

[43] Masato Makino and Masao Doi. Migration of twisted ribbon-like particles in simple shear flow. *Physics of Fluids*, 17:103605, 2005.

[44] Robert L. Carter. *Molecular Symmetry and Group Theory*. John Wileys & Sons, 2000 ?

[45] Jacob Riseman and John G. Kirkwood. The intrinsic viscosity, translational and rotatory diffusion constant of rod-like macromolecules in solution. *The Journal of Chemical Physics*, 18(4):512, 1950.

[46] M Doi and S.F. Edwards. *The Theory of Polymer Dynamics*. Oxford University Press, 1986.

[47] Bruce Alberts, Alexander Jonhson, Julian Lewis, Martin Raff, Keith Roberts, and Peter Walter. *Molecular Biology of the Cell*. Garland Science, Taylor and Francis, 4th edition, 2002.

[48] Simon H. Tindemans, Rhoda J. Hawkins, and Bela M. Mulder. Survival of the aligned: Ordering of the plant cortical microtubule array. *Phys. Rev. Lett.*, 104(5):058103, Feb 2010.

[49] Jean-Marie Lehn. *Supramolecular Chemistry: concepts and perspectives*. Wiley-VCH, 1995.

[50] Michael K Gilson, James A Given, Bruce L Bush, and J.Andrew McCammon. The statistical-thermodynamic basis for computation of binding affinities: A critical review. *Biophysical Journal*, 72:1047–1069, 1997.

[51] Mihail Mihailescu and Michael K. Gilson. On the theory of noncovalent binding. *Biophysical Journal*, 87:23–36, 2004.

[52] Michael K Gilson and Huan-Xiang Zhou. Calculation of protein-ligand binding affinities. *Annual Review of Biophysics and Biomolecular Structure*, 36:21–42, 2007.

[53] Rhoda J. Hawkins and Tom C. B. McLeish. Coarse-grained model of entropic allostery. *Physical Review Letters*, 93(9):098104, 2004.

[54] Sophie Sacquin-Mora, Emilie Laforet, and Richard Lavery. Locating the active sites of enzymes using mechanical properties. *Proteins: Structure, Functions and Bioinformatics*, 67:350–359, 2007.

[55] Richard Lavery and Sophie Sacquin-Mora. Protein mechanics: a route from structure to function. *Journal of Biosciences*, 32(5):891–898, August 2007.

[56] Thorsten Bogner, Andreas Degenhard, and Friederike Schmid. Molecular recognition in a lattice model: An enumeration study. *Phys. Rev. Lett.*, 93:268108, 2004.

[57] Hans Behringer, Andreas Degenhard, and Friederike Schmid. Coarse-grained lattice model for molecular recognition. *Physical Review Letters*, 97(12):128101, 2006.

[58] Hans Behringer, Andreas Degenhard, and Friederike Schmid. Coarse-grained lattice model for investigating the role of cooperativity in molecular recognition. *Physical Review E (Statistical, Nonlinear, and Soft Matter Physics)*, 76(3):031914, 2007.

[59] Marie-Laure Hisette, Paula Haddad, Thomas Gisler, Carlos Manuel Marques, and André Pierre Schröder. Spreading of bioadhesive vesicles on dna carpets. *Soft Matter*, 4:828–832, 2008.

[60] Gimoon Nam, Marie Laure Hisette, Yuting Liang Sun, Thomas Gisler, Albert Johner, Fabrice Thalmann, André Pierre Schröder, Carlos Manuel Marques, and Nam-Kyung Lee. Scraping and stapling of end-grafted dna chains by a bioadhesive spreading vesicle to reveal chain internal friction and topological complexity. *Phys. Rev. Lett.*, 105(8):088101, Aug 2010.

[61] Joachim Radler and Erich Sackmann. Imaging optical thicknesses and separation distances of phospholipid vesicles at solid surfaces. *Journal de Physique II France*, 3:727–748, 1993.

[62] W Helfrich. Elastic properties of lipid bilayers: Theory and possible experiments. *Zeitschrift fur Naturforschung*, 23C:693, 1973.

[63] Sam Safran. *Statistical Thermodynamics of Surfaces, Interfaces and Membranes.* Addison-Wesley, Reading, MA, 1994.

[64] Luca Peliti. *Fluctuating Geometries in Statistical Mechanics and Field Theory*, chapter Amphiphilic Membranes, Les Houches, Session LXII, 1994, page 195. Elsevier, 1996.

[65] J.-B. Fournier. On the stress and torque tensors in fluid membranes. *Soft Matter*, 3:883 – 888, 2007.

[66] J.-B. Fournier, A. Ajdari, and L. Peliti. Effective-area elasticity and tension of micromanipulated membranes. *Phys. Rev. Lett.*, 86(21):4970–4973, May 2001.

[67] Jean-Baptiste Fournier and Camilla Barbetta. Direct calculation from the stress tensor of the lateral surface tension of fluctuating fluid membranes. *Phys. Rev. Lett.*, 100(7):078103, Feb 2008.

[68] P.M. Chaikin and T.C. Lubensky. *Principle of condensed matter physics.* Cambridge University Press.

[69] T. Bickel, C. Marques, and C. Jeppesen. Pressure patches for membranes: The induced pinch of a grafted polymer. *Phys. Rev. E*, 62(1):1124–1127, Jul 2000.

[70] Steven B. Smith, Laura Finzi, and Carlos Bustamante. Direct mechanical measurements of the elasticity of single dna molecules by using magnetic beads. *Science*, 258:1122, 1992.

[71] John F. Marko and Eric D. Siggia. Stretching dna. *Macromolecules*, 28:8759–8770, 1995.

[72] Peter S Swain and David Andelman. The influence of substrate structure on membrane adhesion. *Langmuir*, 15:8902–8914, 1999.

[73] Donald L Ermak and J.A. McCammon. Brownian dynamics with hydrodynamics interactions. *Journal of Chemical Physics*, 69(4):1352, 1978.

[74] Mark E. Tuckerman, Glenn J. Martyna, and Bruce J. Berne. Molecular dynamics algorithm for condensed systems with multiple time scales. *The Journal of Chemical Physics*, 93(2):1287–1291, 1990.

[75] M. Tuckerman, B. J. Berne, and G. J. Martyna. Reversible multiple time scale molecular dynamics. *The Journal of Chemical Physics*, 97(3):1990–2001, 1992.

[76] Alfred Shapere and Frank Wilczek. Gauge kinematics of deformable bodies. *American Journal of Physics*, 57(6):514–518, 1989.

[77] Rhoda J. Hawkins, Simon H. Tindemans, and Bela M. Mulder. Model for the orientational ordering of the plant microtubule cortical array. *Phys. Rev. E*, 82(1):011911, Jul 2010.

[78] Paul B. Comita, Robert B. Gagosian, Henrianna Pang, and Catherine E. Costello. Structural elucidation of a unique macrocyclic membrane lipid from a new, extremely thermophilic,deep-sea hydrothermal vent archaebacterium, methanococcus jannaschii. *Journal of Biological Chemistry*, 259(24):15234–14241, 1984.

[79] Thierry Benvegnu, Loïc Lemiègre, and Sandrine Cammas-Marion. Archaeal lipids: Innovative materials for biotechnological applications. *European Journal of Chemistry*, 28:4725–4744, 2008.

[80] Harmen P. Dijkstra, Jordan J. Hutchinson, Christopher A. Hunter, Haiyuan Qin, Tomas Salvador, Simon J. Webb, and Nicholas H. Williams. Transmission of binding information across lipid bilayers. *Chemistry - A European Journal*, 13:7215–7222, 2007.

[81] Ole G. Mouritsen. *Life-as a matter of fat: the emerging science of lipidomics.* Springer, 2005.

[82] Thomas Heimburg. *Thermal Biophysics of Membranes.* Wiley-VCH, 2007.

[83] Felix M. Goñi, Alicia Alonso, Luis A. Bagatolli, Rhoderick E. Brown, Derek Marsh, Manuel Prieto, and Jenifer L. Thewalt. Phase diagrams of lipid mixtures relevant to the study of membrane rafts. *Biochim. Biophys. Acta*, 1781:665–684, 2008.

[84] Jiang Zhao, Jing Wu, Frederick A. Heberle, Thalia T. Mills, Paul Klawitter, Grace Huang, Greg Costanza, and Gerald W. Feigenson. Phase studies of model biomembranes: Complex behavior of dspc/dopc/cholesterol. *Biochimica and Biophysica Acta*, 1768:2764–2776, 2007.

[85] S Komura, H Shirotori, P.D. Olmsted, and D Andelman. Lateral phase separations in mixtures of lipids and cholesterol. *Europhysics Letters*, 67(2):321–327, 2004.

[86] Jean Wolff, Carlos M. Marques, and Fabrice Thalmann. A thermodynamic approach to phase coexistence in ternary phospholipid cholesterol mixtures. Submitted, 2010.

[87] Sarah L. Veatch, Olivier Soubias, Sarah L. Keller, and Klaus Gawrisch. Critical fluctuations in domain-forming lipid mixtures. *PNAS*, 104(45):17650–17655, November 2007.

[88] J.P Hansen and I Mac Donald. *Theory of simple liquids*. Oxford Science Publications, 1986.

[89] P.A. Egelstaff. *An Introduction to the Liquid State*. Oxford Science Publications, 2nd edition, 1992.

[90] Ronald Dickman and George Stell. Self-consistent ornstein-zernike approximations for lattice gases. *Physical Review Letters*, 77(6):996, 1996.

[91] David P. Landau and Kurt Binder. *A Guide to Monte-Carlo Simulations in Statistical Physics*. Cambridge University Press, 3rd edition, 2009.

[92] Peter Sollich. Predicting phase equilibria in polydisperse systems. *Journal of Physics: Condensed Matter*, 14:R79–R117, 2002.

[93] A.J Bray. Theory of phase ordering kinetics. *Advances in Physics*, page 358, 1994.

[94] Karin A. Riske, Tatiane P. Sudbrack, Nathaly L. Archilha, Adjaci F. Uchoa, Andre P. Schroder, Carlos M. Marques, Mauricio S. Baptista, and Rosangela Itri. Giant vesicles under oxydative stress induced by a membrane-anchored photosensitizer. *Biophysical Journal*, 97:1362–1370, 2009.

[95] G. Weber, A. P. Schroder, T. Charitat, R. Itri, M. Baptista, and C. M. Marques. in preparation, 2010.

[96] C Jeppesen, JY Wong, TL Kuhl, JN Israelachvili, N Mullah, S Zalipsky, and CM Marques. Impact of polymer tether length on multiple ligand-receptor bond formation. *Science*, 293(5529):465, 2001.

[97] Andre G Moreira and Carlos M Marques. The role of polymer spacers in specific adhesion. *Journal of Chemical Physics*, 120(13):6229, 2004.

[98] Kheya Sengupta and Laurent Limozin. Adhesion of soft membranes controlled by tension and interfacial polymers. *Phys. Rev. Lett.*, 104(8):088101, Feb 2010.

[99] F. Brochard-Wyart and P.G. de Gennes. Adhesion induced by mobile binders: Dynamics. *PNAS*, 99(12):7854–7859, June 2002.

[100] Udo Seifert and Reinhard Lipowsky. Adhesion of vesicles. *Physical Review A*, 42(8):4768, 1990.

[101] Peter G. Wolynes and Deutch J.M. Slip boundary conditions and the hydrodynamic effect on diffusion controlled reactions. *1976*, 65(1):450, Journal of Chemical Physics.

[102] Oleg Krichevsky and Grégoire Bonnet. Fluorescence correlation spectroscopy: the technique and its applications. *Report on Progress in Physics*, 65:251–297, 2002.

[103] Joseph R. Lakowicz. *Principle of fluorescence spectroscopy*. Springer, 3rd edition, 2006.

[104] Bernard Valeur. *Molecular Fluorescence: Principle and Applications*. Wiley-VCH, 2002.

[105] Didier Marguet, Pierre-François Lenne, Hervé Rignault, and Hai-Tao He. Dynamics in the plasma membrane: how to combine fluidity and order. *EMBO Journal*, 25:3446–3457, 2006.